UNIVERSITEIT VAN PRETORIA
UNIVERSITY OF PRETORIA
YUNIBESITHI YA PRETORIA

FRICTION FACTOR CORRELATIONS FOR PERFORATED TUBES AT LOW INJECTION RATES

by

IS Mathebula

Submitted in partial fulfilment of the requirements for the degree

MASTER OF ENGINEERING in Mechanical Engineering

in the

Faculty of Engineering, Built Environment and Information Technology
University of Pretoria

Supervisor Prof JP Meyer

December 2011

Title: Friction Factor Correlations for Perforated Tubes at Low Injection Rates

Author: Ipeleng Samson Mathebula
Student number: 26006741
Study leader: Prof JP Meyer
Degree: Master of Engineering (Mechanical)
Department: Mechanical and Aeronautical Engineering

Abstract

Perforated tubes are widely used in industry for various applications. A special application arises when there is fluid injection into the perforated tube. Such cases arise when perforated tubes are used for horizontal oil well drilling and French drains. The behaviour of the flow under these conditions has led to the development of correlations, which consider the effects of the perforations and injection process. However, there are few friction factor correlations in literature, which consider the increased kinetic energy at the perforated tube outlet caused by fluid injection and acceleration. The current study reports experimental correlations for determining the friction factor of perforated tubes when the additional kinetic energy from the injection process is considered. The friction factor measurements were conducted in copper tubes with an internal diameter of 20.8 mm and a wall thickness of 1 mm at three non-dimensional pitches of 0.375, 0.75 and 1.5. A perforated length-to-diameter ratio of 40:1 was used for the perforated tubes. A perforation row contained seven small perforation holes with a diameter of 1.5 mm spaced evenly around the perimeter of the tube. These perforation rows were staggered row to row, resulting in triangular perforation patterns. Water was used as a test medium with Reynolds numbers at the tube outlet ranging from 20 000 to 60 000. The injection ratio was varied from 0 to 5% to obtain a total of 135 unique combinations of perforated tube friction factor data at different injection ratios, Reynolds numbers and non-dimensional perforation pitches. The experiments were condensed into friction factor correlations, which allow perforated tube parameters to be optimisation for minimising pressure losses encountered in draining operations.

Keywords: perforated tubes, friction factor, friction reduction, draining

Acknowledgements

I thank God for all the people that have been around me while undertaking this research. I would like to thank Professor JP Meyer, for affording me the freedom of selecting my own research topic and affording me his expertise and resources. I am grateful for the CSIR, for the financial, technical and administrative support, which proved invaluable for the duration of the study. I also extend my gratitude to Danie Gouws and Koos Mthobeni for teaching me the practical aspects of conducting lab work.

The funding obtained from the NRF, TESP, Stellenbosch University, University of Pretoria, SANERI/SANEDI, CSIR, EEDSM hub and NAC is acknowledged and duly appreciated.

Table of Contents

Abstract i
Acknowledgements ii
List of Figures v
List of Tables vii
List of Symbols viii

1. Introduction 1
1.1 Background 1
1.2 Purpose of the Study 4
1.3 Overview 4

2. Literature Study 5
2.1 Introduction 5
2.2 Pressure Drop 5
2.2.1 Background 5
2.2.2 Friction Factor Correlations 6
2.3 Perforated Tubes 7
2.4 Summary 11

3. Experimental Set-up 12
3.1 Introduction 12
3.2 Equipment and Instrumentation 12
3.3 Test Section and Perforated Tube 14
3.4 Scope of Experiments 17
3.5 Data Acquisition and Reduction 18
3.6 Calibration and Uncertainty 19
3.7 Validation and Verification 21
3.7.1 Test Set-up Validation 21
3.7.2 Injection System Verification 22
3.8 Summary 23

Table of Contents (continued)

4. Experimental Results 24
4.1 Introduction 24
4.2 Zero Injection Friction Factor 24
4.3 Injection Friction Factor 25
4.4 Summary 28

5. Discussion 29
5.1 Introduction 29
5.2 Friction Factor Correlations 29
5.3 Fluid Acceleration Correction 32
5.4 Application 34
5.4.1 Example 1 34
5.4.2 Example 2 38
5.5 Summary 39

6. Conclusion and Recommendations 40
6.1 Summary 40
6.2 Conclusions 42
6.3 Recommendations 42

7. References 43

List of Figures

Figure 1: Horizontal oil well drilling with a perforated pipe 1
Figure 2: Cross section of French drains with a perforated pipe 2
Figure 3: Lateral inflow into 10-segments of a perforated tube test section Siwoń of (1987).. 3
Figure 4: Equilateral triangle or staggered perforation pattern Siwoń (1987) 3
Figure 5: Flow through a plain tube with a stationary wall adopted from White (2008) 5
Figure 6: Flow through a perforated tube with a stationary wall adopted from White (2008) . 8
Figure 7: Perforation nozzle effect 10
Figure 9: Schematic representation of experimental set-up 12
Figure 10: Mounting of thermocouples adopted from Meyer and Olivier (2011) 13
Figure 11: A photograph of the experimental facility and equipment..... 14
Figure 12: Method of test section construction and completed test sections 15
Figure 13: Definition of perforated tube and test section..... 16
Figure 14: Variation in perforation pattern longitudinal spacing 17
Figure 15: Summary of the scope of the experiments 18
Figure 16: Experimental set-up validation with the aid of a plain tube without any perforation holes 22
Figure 17: Injection system verification with the aid of fine pitch friction factor data in the absence of injection..... 23
Figure 18: Friction factors against Reynolds number for a plain tube and for all the perforated tube patterns in the absence of fluid injection 25
Figure 19a: Friction factor against Reynolds number for a plain tube and a fine pitch perforation pattern at different injection ratios..... 26
Figure 19b: Friction factor against Reynolds number for a plain tube and a medium pitch perforation pattern at different injection ratios 26
Figure 19c: Friction factor against Reynolds number for a plain tube and a coarse pitch.....27
Figure 20: Friction factor against injection ratio for a fine pitch perforation pattern at Reynolds numbers of 20 000, 40 000 and 60 000 27
Figure 21: Measured friction factor against predicted friction factor in the absence of injection for the fine, medium and coarse pitch perforation patterns 30

List of Figures (continued)

Figure 22: Linear increase in friction factor against injection ratio for a fine pitch perforation pattern at Reynolds numbers of 20 000, 40 000 and 60 000 31
Figure 23: Measured friction factors with fluid injection against predicted friction factors at a Reynolds number of 40 000 for the fine, medium and coarse perforation patterns 31
Figure 24: Fluid acceleration correction term against injection ratio at length-to-diameter ratios of 20, 40 and 60 32
Figure 25: Effect of fluid acceleration correction term on the calculated friction factors with varying injection ratios for the fine, medium and coarse pitch perforation patterns at a Reynolds number of 40 000 33
Figure 26: Schematic representation of Example 1 35
Figure 27: Outline of seven-step length segmentation method 35
Figure 28: Schematic representation of the segmented low injection version of Example 1 . 36
Figure 29: Influence of a diffuser on the friction factor of local segments along the length of a perforated tube which is divided into 10-segments 38

List of Tables

Table 1: Common turbulent friction factor correlations adopted from White (2008) 7
Table 2: Dimension of perforated tube and test section..... 16
Table 3: Properties and features of the perforation patterns 17
Table 4: Measured variables and calibration factors 20
Table 5: Measurement range and uncertainty..... 20
Table 6: Experimental range and maximum uncertainty 21
Table 7: Zero injection friction factor prediction constants..... 29
Table 8: Segmented low injection solution for Example 5.1 36
Table 9: Friction factor compensation constants for accounting for the plain tube sections .. 37
Table 10: Influence of the fluid acceleration correction term per segment due to a diffuser . 39

List of Symbols

Alphabetical symbols

Symbol	Description	SI units
a	Constant	[-]
a_β	Geometric progression ratio	[-]
b	Constant	[-]
c	Constant	[-]
c_e	Coefficient	[-]
d	Perforation diameter	[m]
D	Diameter	[m]
E	Error	[-]
f	Friction factor	[-]
f_D	Friction factor with a diffuser	[-]
f_l	Literature friction factor	[-]
f_o	Zero injection friction factor	[-]
Δf	Friction reduction correction term	[-]
g	Gravitational acceleration	[m/s^2]
h_f	Head loss factor	[m]
i	Data point counter	[-]
j	Segment counter	[-]
k	Secondary segment counter	[-]
l_1	Length of first segment	[m]
lj	Length of segment j	[m]
L	Tube or test length	[m]
L_1	Tube entrance length	[m]
L_2	Perforation entrance length	[m]
L_3	Perforation length	[m]
L_4	Perforation exit length	[m]
L_5	Tube exit length	[m]
m	Gradient	[-]
n	Number of perforations	[-]

List of Symbols (continued)

Alphabetical symbols

Symbol	Description	SI units
OD	Outer diameter	[m]
p	Perforation pitch	[m]
P	Injection pressure	[Pa]
P_1	Inlet pressure	[Pa]
P_2	Outlet pressure	[Pa]
ΔP	Pressure drop	[Pa]
ΔP_D	Pressure drop with a diffuser	[Pa]
ΔP_k	Acceleration pressure drop	[Pa]
P/D	Pitch diameter ratio	[-]
q	Injection flow rate	[m^3/s]
q_j	Injection flow rate for segment j	[m^3/s]
q_k	Injection flow rate for segment k	[m^3/s]
Q	Inlet flow rate	[m^3/s]
Q_o	Outlet flow rate	[m^3/s]
Q_{oj}	Outlet flow rate for segment j	[m^3/s]
Re	Reynolds number	[-]
r	Assumed injection ratio	[-]
r_j	Injection ratio for segment j	[-]
r_Q	Injection ratio	[-]
s	Number of segments	[-]
T	Temperature average	[°C]
T_1	Thermocouple reading 1	[°C]
T_2	Thermocouple reading 2	[°C]
T_3	Thermocouple reading 3	[°C]
T_4	Thermocouple reading 4	[°C]
V	Average flow velocity	[-]
V_1	Inlet velocity	[m/s]
V_2	Outlet velocity	[m/s]

List of Symbols (continued)

Greek symbols

Symbol	Description	SI units
α	Perforation kinetic energy correction term	[-]
α_1	Inlet kinetic energy correction term	[-]
α_2	Outlet kinetic energy correction term	[-]
β	Arbitrary parameter	[-]
$\bar{\beta}_m$	Measured arbitrary parameter	[-]
β_o	Arbitrary parameter offset	[-]
ε	Wall roughness	[m]
ϕ	Porosity	[-]
μ	Fluid viscosity	[-]
ρ	Fluid density	[kg/m^3]
τ_w	Wall shear stress	[Pa]

1. Introduction

1.1 Background

There are numerous applications for perforated tubes in the commercial environment. Perforated tubes can be found in commercial buildings or homes with stylish perforation patterns for aesthetic purposes. Some perforation patterns are designed for damping specific frequencies in exhaust mufflers. Common pipes are sometimes customised into perforated pipes for irrigation purposes by simply drilling multiple holes. Singh and Rao (2009) demonstrated that the design of perforation patterns is also critical for the performance of pressurized heavy water reactors.

An interesting application of perforated tubes arises when there is fluid mixing and lateral fluid inflow. The mixing may involve two different chemical species as in the case of air and fuel for combustion in burners. Other processes involve the mixing of a homogeneous fluid at different temperatures for film cooling or temperature regulation.

Horizontal oil well drilling investigated by Dikken (1990) and other researchers is another example where there is fluid injection into perforated tubes. Fluid injection during horizontal oil well drilling (Figure 1) is crucial for a successful operation because lateral inflow takes full advantage of the increased surface area, which is made available by the orientation of the drilling operation.

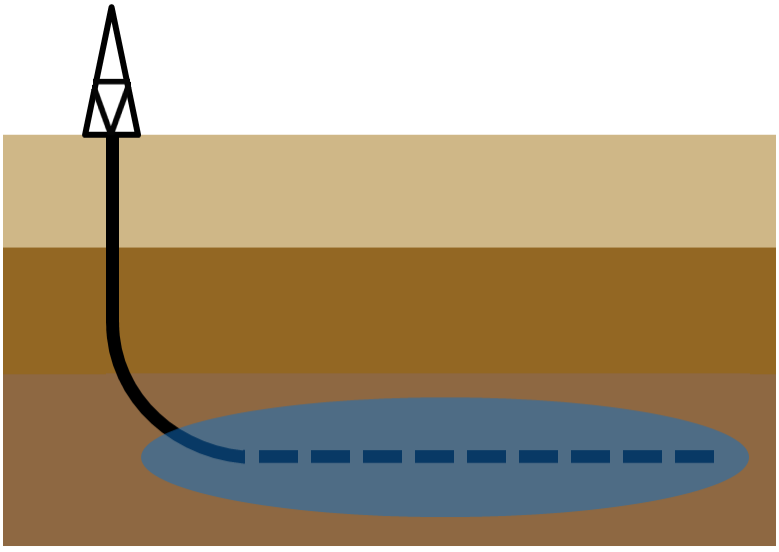

Figure 1: Horizontal oil well drilling with a perforated pipe

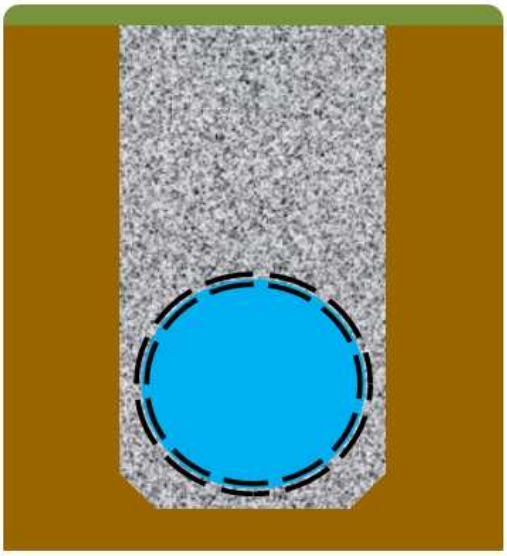

Figure 2: Cross section of French drains with a perforated pipe

Horizontal oil well drilling is a large-scale draining operation and shares its technology with a simpler French drain design. The French drain pictured in Figure 2 consists of a perforated pipe buried in gravel and lateral inflow is used for directing groundwater away from water-sensitive areas in the garden. Hence, the draining problems encountered by landscape designers overlap with those experienced by petrochemical engineers since both problems involve draining a fluid by lateral inflow into a perforated pipe. Thus, the solutions which are available in literature are contributions from both industries.

Clemo (2010) revisited the lateral inflow solutions of Siwoń (1987), when developing a borehole simulation program and found results, which were in good agreement with the latter researcher's work. Siwoń (1987) conducted experiments on perforated tubes with water as a test medium. The tests were conducted in the turbulent regime with Reynolds numbers ranging from 9 680 to 125 830 and injection Reynolds numbers varying from 13 to 4 562. The perforated pipes were made from PVC with an internal diameter of 56.6 mm and a wall thickness of 5 mm. A perforated length-to-diameter ratio of 80:1 was employed to ensure fully developed flow in the perforated pipe. The perforated pipes were housed in an annulus manufactured from 10 independent segments and each segment measured 460 mm in length with an outer diameter of 114 mm. A schematic representation of the test section is depicted in Figure 3.

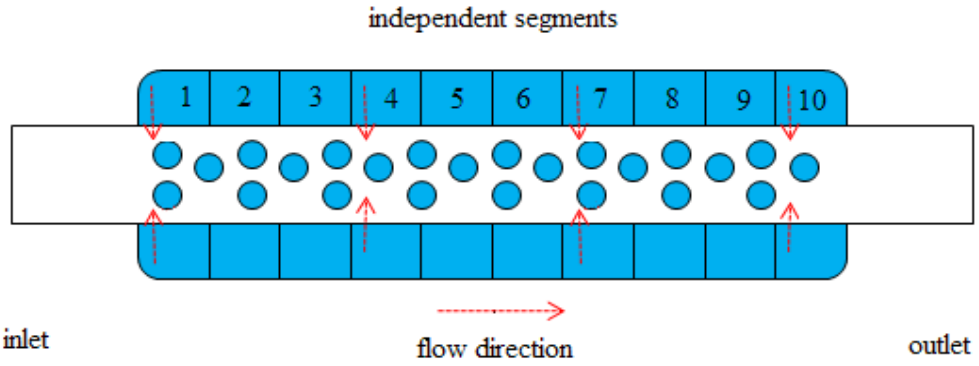

Figure 3: Lateral inflow into 10-segments of a perforated tube test section Siwoń of (1987)

Nine perforated pipes with different perforation patterns and orifice diameters were tested. The perforation patterns formed equilateral triangle patterns or staggered pattern as shown in Figure 4. The flow inside the perforated tube approached the pattern from left to right as indicated by the red arrow. The first row of perforations formed the base of the equilateral triangle and the height of the triangle was the perforation pitch, *p*. Siwoń (1987) used porosity and perforation diameter to specify a perforation pattern. Three orifice diameters of 4.5, 6 and 9 mm were used at three different porosity values to obtain nine different perforation patterns.

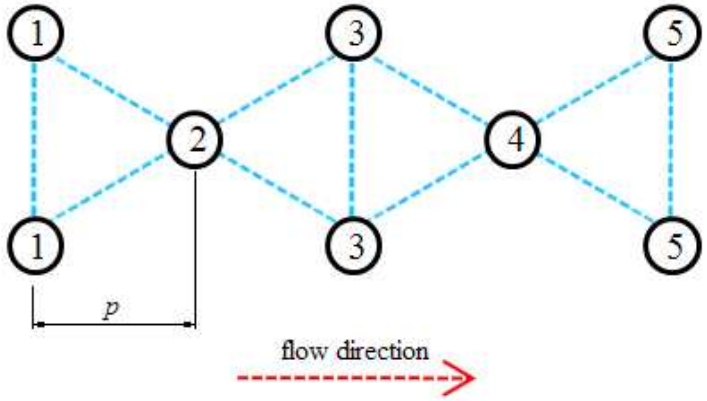

Figure 4: Equilateral triangle or staggered perforation pattern Siwoń (1987)

Measurements indicated an artificial roughening effect due to the presence of the perforations when injection was absent. The roughening effect, also known as perforation roughness, was proportional to the porosity and was increased by either increasing the perforation diameter or porosity of the perforation pattern. Additional measurements with injection revealed an increase in pressure drop with an increase in injection rate. Thus, the pressure drop measured across perforated pipes was always higher than those of smooth pipes under the same flow conditions.

Su and Gudmundsson (1998) conducted similar experiments but with a different perforation pattern. The perforation pattern had a pitch of 25.4 mm and a phasing of 60°. The recorded measurements agreed with those in literature and then the authors went a step further by describing separate pressure drop terms, which sum to the measured pressure drop. The suggested pressure drop terms were friction, perforations roughness, fluid mixing and acceleration pressure drop components. The pressure drop caused by perforation roughness and fluid mixing were lumped together and classified as additional losses. The additional losses pressure drop term was obtained from the measured pressure drop after subtracting the pressure drop contribution due to wall friction and fluid acceleration. The modified results indicated a reduction in additional pressure drop with an increase in injection. Su and Gudmundsson (1998), then presented these results as a pressure loss coefficient for injection ratios spanning from 0% to 35%.

There have been a few attempts in literature to repeat the experiments of Siwoń (1987), in the light of the insight given by Su and Gudmundsson (1998). The reduction in friction outlined by the latter authors was also spread over a large injection ratio range with a low resolution of the data. In addition to the low resolution, the pressure loss coefficient was not expressed in the familiar friction factor form used for plain tubes.

1.2 Purpose of the Study

The purpose of this study is to measure the friction factor of three different perforation patterns at low injection ratios, lower than those of Siwoń (1987), and develop friction factor correlations which have the ability to account for the effects of fluid acceleration such that the pressure drop across perforated tubes with injection can be quantified in a familiar friction factor form with improved low injection ratio resolution.

1.3 Overview

The remainder of the dissertation is divided into four chapters and a conclusion. The literature study (Chapter 2), experimental set-up (Chapter 3), experimental results (Chapter 4) and friction factor correlations (Chapter 5) are presented and the dissertation is concluded in Chapter 6.

2. Literature Study

2.1 Introduction

The literature chapter commences with describing the pressure drop, which occurs across a plain tube with uniform diameter. The laws of conservation of mass and momentum were applied to introduce friction factor as a dimensionless pressure drop. The three main flow regimes encountered in practice were classified in terms of the Reynolds number. Common turbulent friction factor correlations were given and the limitations of common turbulent friction factor correlations for determining the friction factors of perforated tubes were demonstrated by reapplying the laws of conservation to a perforated tube example. The relevance of the work of Siwoń (1987), and Su and Gudmundsson (1998) was explained by comparing the published correlations with the equation obtained from the perforated tube example.

2.2 Pressure Drop

2.2.1 Background

The pressure drop measured across a plain tube with a uniform diameter is caused by the no-slip boundary condition, which exists between the stationary tube wall and the adjacent moving fluid. The modified Bernoulli equation expressed in equation (2.1) describes the conservation of the momentum of the system and includes a head loss term, h_f, to account for the irreversible pressure losses due to wall friction caused by the no-slip boundary condition.

$$P_1 + \frac{1}{2}\rho\alpha_1 V_1^2 = P_2 + \frac{1}{2}\rho\alpha_2 V_2^2 + \rho g h_f \tag{2.1}$$

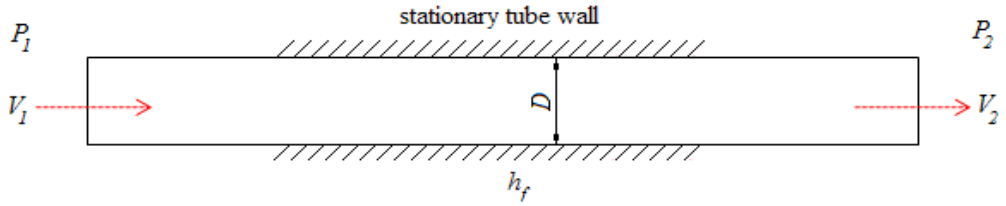

Figure 5: Flow through a plain tube with a stationary wall adopted from White (2008)

The modified equation can be rearranged by grouping the pressure terms and isolating the remaining terms on the right hand side as in equation (2.2). The inlet and outlet velocity terms fall away when enforcing the law of conservation of mass with fully developed flow. Weisbach (White, 2008) used equation (2.3) to introduce friction factor in the place of head losses such that the pressure drop is dimensionless parameter.

$$P_1 - P_2 = \rho g h_f + \frac{1}{2}\rho(\alpha_2 V_2^2 - \alpha_1 V_1^2) \tag{2.2}$$

$$P_1 - P_2 = \frac{fL}{D}\frac{\rho V^2}{2} \tag{2.3}$$

White (2008) also expressed friction factor as a function of the wall shear stress with equation (2.4). The direct relationship between friction factor and shear stress relates the measured pressure drop to shear stresses. Hence, pressure drop and friction factor are indirect methods for predicting the magnitude of the wall shear stress as observed by Rohr et al. (1992). However, errors are introduced if wall shear stresses and losses are determined from pressure when a fluid is injected through the boundary layer.

$$f_l = \frac{8\tau_w}{\rho V^2} \tag{2.4}$$

2.2.2 Friction Factor Correlations

Friction factor correlations are classified by the behaviour of the flow as specified by the Reynolds number. The Reynolds number is a dimensionless flow speed defined by equation (2.5) and most flows which are encountered in engineering practice can be classified into one of the three major flow regimes depending on the Reynolds number. These flow regimes are laminar, transition and turbulent flow. Laminar flow is distinguished by smooth and ordered streamlines with Reynolds numbers ranging between 100 and 1 000 while turbulent flow exhibits random and fluctuating streamlines. Fully turbulent flows are observed at Reynolds numbers exceeding 10 000 and transitional flow is a hybrid of laminar and turbulent flow. Transitional flow commences at upper Reynolds numbers of laminar flow and becomes fully turbulent at Reynolds numbers exceeding 10 000.

$$Re = \frac{\rho V D}{\mu} \tag{2.5}$$

The friction factors in the laminar regime are predicted by the well-known Poiseuille equation (White, 2006). The Pouseille equation is only valid in the laminar regime and fails to account for the flow fluctuations, which are present in both transitional and turbulent flows. It was accepted that the transition from laminar to turbulent occurs at a Reynolds number of 2 300 (Meyer and Olivier, 2011), but the authors indicated that transition depends on entrance effects. The latter authors also added to the efforts of Ghajar and Tam (1997) in increasing the depth of friction factor literature in the transitional regime. Turbulent friction correlations are suitable for predicting friction factors at Reynolds numbers exceeding 10 000 and Table 1 tabulates some of the well-known correlations (White, 2008).

	Name	Year	Equation	Equation
1	Blasius	1911	$f_l = 0.316\, Re^{-0.25}$	(2.6)
2	Prandtl	1935	$f_l = \left[\frac{1}{2.0\log(Re\, f_l^{0.5}) - 0.8}\right]^2$	(2.7)
3	Colebrook	1939	$f_l = \left[-2.0log\left(\frac{\varepsilon/D}{3.7} + \frac{2.51}{Re\, f_l^{0.5}}\right)\right]^{-2}$	(2.8)
4	Haaland	1983	$f_l = \left[-1.8log\left(\frac{6.9}{Re} + \left(\frac{\varepsilon/D}{3.7}\right)^{1.11}\right)\right]^{-2}$	(2.9)

Table 1: Common turbulent friction factor correlations adopted from White (2008)

2.3 Perforated Tubes

The modified Bernoulli equation used for plain tubes without any perforations is applied again to the perforated tube with fluid injection (figure 6). The figure illustrates perforations of diameter, *d*, with flow injected at a rate, *q*, at an injection pressure, *P*. The flow energy entering the perforated tube through all the perforations is added as the third term seen on the right-hand side of equation (2.10). The third term is due to fluid inflow and falls away when injection and perforation are absent such that equation (2.10) reverts to equation (2.2). Hence, it can be argued that perforations and injection must alter the pressure drop and the corresponding friction factors in perforated tubes due to radial inflow.

$$P_1 - P_2 = \rho g h_f + \frac{1}{2}\rho(\alpha_2 V_2^2 - \alpha_1 V_1^2) - \left[P + 2\frac{\rho\alpha q}{d^2\pi}\right] \tag{2.10}$$

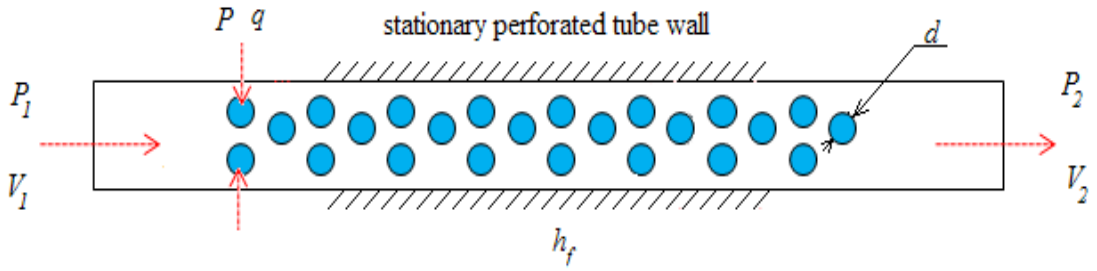

Figure 6: Flow through a perforated tube with a stationary wall adopted from White (2008)

Equation (2.10) does not always converge to equation (2.2) in the absence of injection. Kays (1971), explained that pores or perforations with a diameter and/or spacing which is larger than the laminar sublayer will act as artificial roughening in the absence of injection. An alternative argument was posed in the form of kinetic energy correction factors given by White (2008). The momentum equation of perforated tubes with no injection takes the form of equation (2.11) since the inlet and outlet velocities are equal. The kinetic energy term does not reduce to zero unless the perforations are sufficiently small. The diameters and spacing of perforated tube patterns are often large enough to distort the velocity profile and cause different kinetic energy correction terms at the inlet and outlet. In such a case, the kinetic energy term would not fall away and the pressure drop would be higher than those experienced in plain tubes. Hence, common turbulent friction factors are insufficient to describe the effect of perforation roughness. The comments made by White (2006), based on experimental data, also agree with these observations.

$$P_1 - P_2 = \rho g h_f + \frac{1}{2}\rho V^2(\alpha_2 - \alpha_1) \tag{2.11}$$

A further deviation from plain tube flow behaviour exists when fluid injection is present. The flow in perforated tubes differs from conventional pipe flow as there is radial fluid inflow through the perforations. The injection disturbs the velocity profile and boundary layer (Kato et al, 1998) such that the pressure gradient along the length of the perforated tube is affected. Boundary layer injection reduces the friction of the surface the wetted surface. This effect was observed clearly in the transpiration experiments of Kays (1971) and Eckert et al. (1973). The reduction in friction for transpiration experiments was proportional to the rate of fluid injection and the reduction in friction was more pronounced for porous surfaces since the average diameters of the surface are sufficiently small. The last term on the right hand side illustrates qualitatively that increasing injection rate, *q*, for surfaces with a small perforation diameter, *d*, will yield greater reductions in pressure losses.

The second term in equation (2.10) is referred to as the kinetic energy or fluid acceleration term. This term exhibits different characteristics depending on the nature of the flow. Kays (1971) studied the influence of external and internal flows in order to describe the behaviour of the acceleration term. The cases involved constant free-stream and accelerated boundary layers cases. The reduction in pressure drop and friction factor was obvious for the constant free-stream case since the free-stream velocity of external flows remains fairly constant outside of the boundary layer. The varying free-stream results became difficult to quantify and inconclusive remarks were reported.

Lateral injection in perforated tubes clarified the behaviour of the acceleration term for varying free stream cases observed by Kays (1971). Fluid acceleration in perforated tubes studies was achieved by continuously injecting fluid along the length of the perforated tubes. Thus, the flow conditions are classified as internal flow. The variables driving the measured pressure drop under for perforated tubes with injection were friction and perforation roughness losses, as well fluid acceleration and mixing pressure drop terms (Su and Gudmundsson, 1998). The former pair of variables are characterised in the absence of fluid injection while fluid acceleration and mixing exist only when injection is present.

Fluid mixing occurs in the proximity of the perforation where injection occurs (Rathgeber and Becker, 1983). Each perforation with injection acts as jet that disturbs the flow locally and the mixing effects diminish over lengths, which are much shorter when compared to the overall perforated length. On the other hand, fluid acceleration takes place over the entire length of the perforated tube as opposed to mixing, which is limited to the section downstream of each perforation. Fluid acceleration can be described by the nozzle effect, which is driven by the law of conservation of mass.

The nozzle effect can be described graphically with the aid of Figure 7. The total area of the blue circles represents the area of the inlet while the red circle area represents the outlet. An area ratio, which is not equal to unity, implies that an incompressible fluid will be accelerated as it flows from the inlet to the outlet. Accelerating the fluid causes the outlet pressure to be marginally lower. This reduced outlet pressure is automatically incorporated into the experimental measurements. Hence, it is necessary to correct for fluid acceleration since the nozzle effect would exaggerate the measured pressure drop and over predict the losses measured when injection is present.

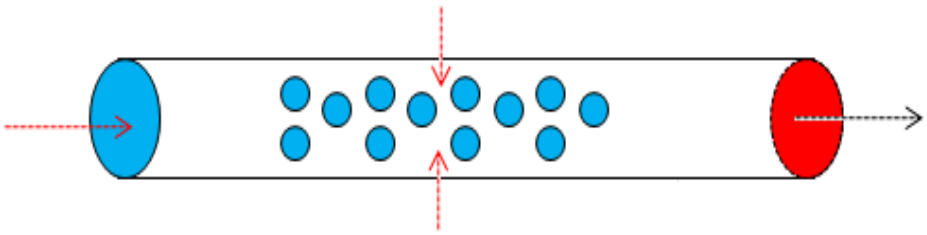

Figure 7: Perforation nozzle effect

Siwoń made use of equation (2.12) to describe fluid acceleration in perforated tubes. The kinetic energy correction terms were collapsed into a single coefficient, c_e, which ranges between 1.05 and a maximum of 1.86. These solutions predict an increase in pressure drop with an increase in injection rate and the results were also verified by Clemo (2010).

$$\Delta P_k = \frac{1}{2} c_e \rho (V_2^2 - V_1^2) \tag{2.12}$$

In 1998, Su and Gudmundsson performed similar experiments to Siwoń (1987). A schematic representation of their experimental set-up is shown in Figure 8. The tube was divided into two equal sections containing the perforated and plain sections. The tube had a diameter of 21.94 mm and each section measured 600 mm in length. The pitch of the perforations was 25.4 mm with a perforation diameter of 3 mm. Each row contained six perforations spaced evenly around the perimeter of the tube. The injection system was more simplified in comparison with that of Siwoń (1987). The injection system was made from a single water jacket with an internal diameter of 190 mm. The water in the jacket flowed in parallel with the water in the perforated tube and a large annular ratio of 6.3 was used to obtain uniform pressure distribution in the annulus. The rate of inflow into the perforations was regulated by means of a 20-micron filter, which covered the perforations.

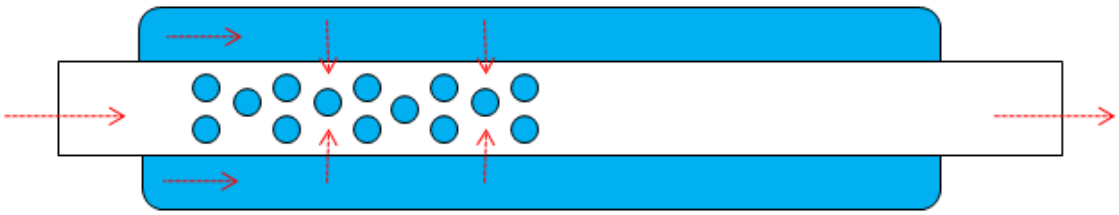

Figure 8: Schematic representation of the injection system of Su and Gudmundsson (1998)

The experiments were conducted in the turbulent flow regime with Reynolds numbers ranging from 37 000 to 95 000 and the injection ratios spanned from 0% to 35%. The authors also reported an increase in pressure drop with an increase in injection rate. However, they subsequently subtracted the kinetic energy term from the measured pressure drop after assuming the energy is recovered through an ideal diffuser. Thus, a coefficient, c_e, of 2 was used instead of the maximum value recommended by Siwoń. The adjusted results indicated a reduction in wall friction losses as the injection rate was increased. These solutions resolved the contradictions of Kays' (1971) transpiration results and proved that injection alters the shear stress and skin friction in perforated tubes when there is fluid acceleration.

2.4 Summary

The pressure drop experienced across plain tubes can be computed from a relevant friction factor correlation when the Reynolds number and flow regime are known. However, these correlations are inaccurate for predicting the friction factor and pressure drop of perforated tubes since the effects of perforation roughness and injection are not taken into account by common friction factor correlations. Perforation roughness is caused by the relatively large perforation diameters and spacing, which are an intrinsic trait of perforated tubes. Fluid injection causes further discrepancy by introducing a secondary term, which influences the pressure drop across the perforated tube. The additional term changes the momentum balance across the perforated tube through a mechanism of boundary layer distortion. Injection distorts the boundary layer in such a manner that the friction and pressure drop across the surface are reduced but perforated tube experimental results indicate contradictory effect. Fluid acceleration was seen as the main culprit for causing the increase in pressure drop with an increase in injection. These effects were reversed by subtracting the kinetic energy term associated with fluid acceleration. The pressure drop reduction results, which are available in literature for perforated tubes were obtained after subtracting an ideal kinetic energy term and the injection losses effects of other researchers were not considered. Therefore, it is desirable to remove the ideal assumption and then apply the available knowledge to refine the method of determining the friction factor and pressure drop across perforated tubes with fluid injection.

3. Experimental Set-up

3.1 Introduction

The experimental equipment and instrumentation used for the measurements are described in the first section to give a background of the equipment and instruments used to conduct the experiments. Then the construction of the test sections is explained in the subsequent section. The following section discusses the dimensions of the perforated tube and the geometry of the perforation patterns. The Reynolds number and injection ratio ranges used for experiments are reported under the scope of experiments. The data reduction method and calibration factors are described in the fourth section. The fifth section gives a brief report of the uncertainties of the present study and the validation and verification of the experimental set-up and injection system are reported in the last section of the chapter.

3.2 Equipment and Instrumentation

The experimental set-up and equipment for conducting the experiments were housed in the Thermoflow Laboratory at the University of Pretoria. A schematic representation of the experimental set-up is shown in Figure9 with the main flow line with a flow rate, *Q*, and the injection line with flow rate, *q*. The experimental set-up consisted of a water reservoir (1), pumps and accumulators (2), rotameters (3), Coriolis flow meters (4), filters (5), perforated tube test section (6) and a flow mixer (7), which was used for measuring the water temperature to obtain fluid properties at the test section outlet.

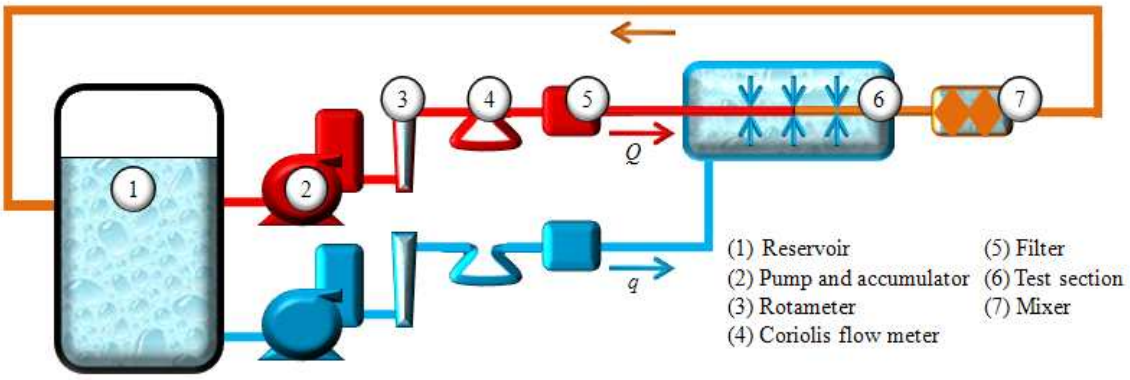

Figure 9: Schematic representation of experimental set-up

The reservoir had a capacity of 600 *l* and fed water with a centrifugal pump to the main line, which flowed through the inner tube of the test section. A positive displacement pump fed water from the same reservoir to the annulus of the test section where the water was radially injected into the inner tube. Accumulators were installed in the flow lines to damp flow pulsations. The injection and main line made use of 4 *l* and 20 *l* accumulators respectively.

The flow rates in the two lines were measured with Coriolis flow meters. Rotameters were used in series with the Coriolis flow meters for validation purposes. A plain tube without any perforations was connected in parallel with the perforated tube for validation purposes. Two 100-micron disc filters were installed in the lines to prevent the perforations from being blocked. A mixer with four T-type thermocouples (Figure 10) mentioned in Meyer and Olivier (2011) was installed on the tube outlet for measuring the average water temperature, which was then used to determine the density and viscosity of the water. A calibrated differential pressure transducer was used for measuring the pressure drop across the test length of the tubes.

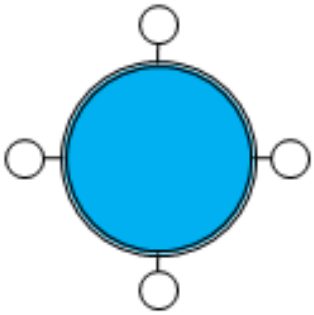

Figure 10: Mounting of thermocouples adopted from Meyer and Olivier (2011)

The experimental set-up was also furnished with two amplifiers. A voltage amplifier was used for pressure drop measurements and a current amplifier for flow measurements. Either the main or injection flow rate meter readings were amplified since a single current amplifier was available. The selection of either flow meter was achieved from a selector circuit. Hence, there was a delay between the flow rate measurements of the main and injection lines. A total of six channels were measured and fed to a data acquisition system. Four channels were occupied by temperature readings from the mixer along with a single voltage channel for pressure drop readings. The last channel in the data acquisition system was reserved for flow rate measurements. Figure 11depicts the Thermoflow Laboratory as well as the experimental set-up together with the data logging equipment.

Figure 11: A photograph of the experimental facility and equipment

3.3 Test Section and Perforated Tube

Test Section

The test sections were made from copper using standard tubes and fittings. The tubes and fittings were joined together by the lead-tin soldering technique. Figure 12 illustrates the construction process and completed test sections. The simpler tube-in-tube injection system with parallel flow of Su and Gudmundsson (1998) was adopted for the present study. However, a smaller annular ratio was employed over the larger annular ratio as injection mass flow rates were much lower. Hence, the filter for covering the perforations could be omitted.

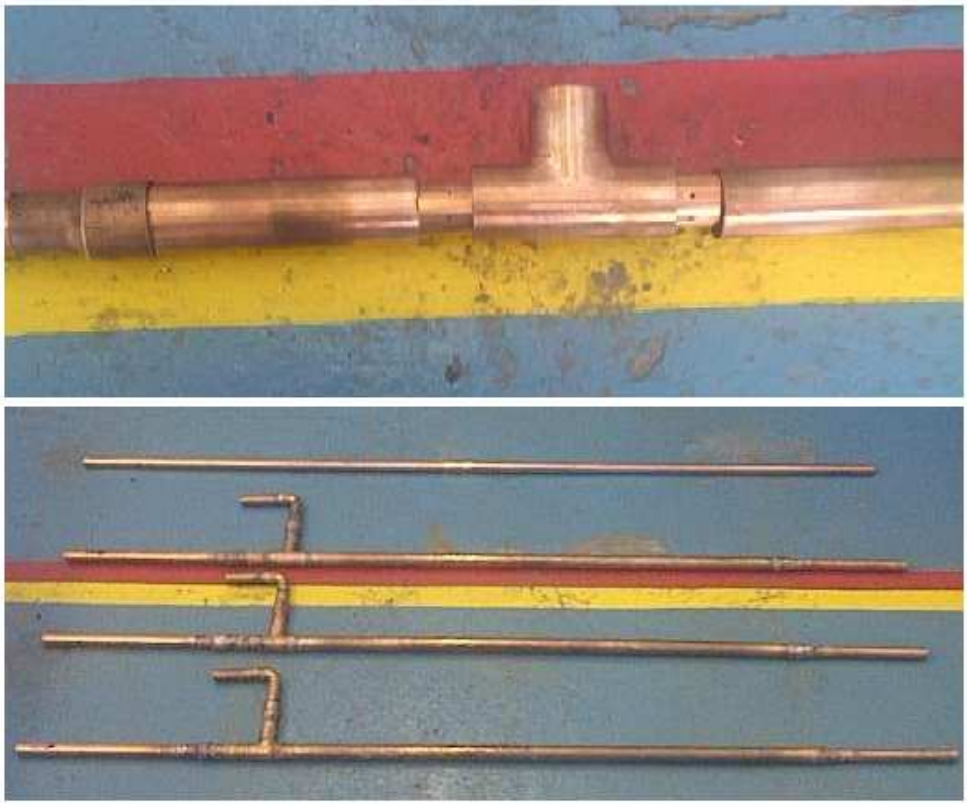

Figure 12: Method of test section construction and completed test sections

Perforated Tube and Pattern

The perforated tubes were manufactured from hard-drawn copper tubes with an outer and inner diameter of 22 mm and 20.8 mm respectively. The perforated tube had a total length of 1.7 m and was divided into five segments as shown in Figure 13. The segments were the entrance length, L_1, perforation entrance length, L_2, perforated length, L_3, perforation exit length, L_4, and exit length, L_5. The dimensions of the segments are listed in Table 2. The pressure drop was measured across the test length, L, of 1.225 m with pressure taps, which have a diameter of 1 mm. The procedure for preparing the test sections and pressure taps was similar to the process implemented by Meyer and Olivier (2011). The major deviation from the method of the previous authors was the provision made to the entrance and exit lengths. The entrance length was adjusted to 12.5 hydraulic diameters for ensuring fully developed flow. The entrance length was longer when compared with the 10 hydraulic diameters suggested in White (2008). The length of 10 hydraulic diameters was used as an entrance length to the perforated length and as an exit length of the entire perforated tube.

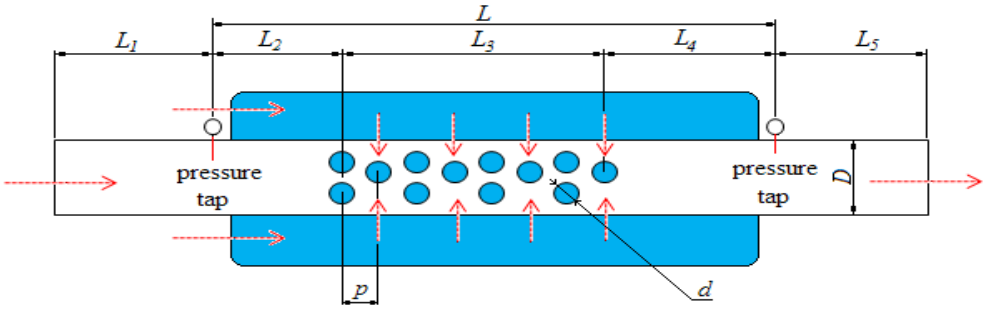

Figure 13: Definition of perforated tube and test section

	Parameter	Symbol	Size [mm]
1	Tube entrance length	L_1	250
2	Perforation entrance length	L_2	200
3	Perforation length	L_3	800
4	Perforation exit length	L_4	250
5	Tube exit length	L_5	200
6	Test length	L	1225
7	Perforation diameter	d	1.5
8	Inner diameter	D	20.8
9	Outer diameter	OD	22

Table 2: Dimension of perforated tube and test section

Three perforation patterns with perforation diameter of 1.5 mm were prepared by varying the perforation pitch of the tubes. The tubes were graded fine, medium and coarse according to the length of the pitch. The fine tube perforation pattern was derived from the equilateral triangle perforation pattern of Siwoń (1987). The perforation pattern had seven holes spaced evenly around the perimeter of the tube and the perforation pattern extended for a length of 800 mm. The pitch of the fine pattern was 7.8 mm and the pattern is shown in blue in Figure 14. The medium and coarse patterns were variations of the fine pattern stretched in the direction of the flow. The medium and coarse perforation patterns are shown in red and black respectively in the same figure. The pitches of the medium and coarse patterns were 15.6 mm and 31.2 mm respectively. The pitch, p, pitch-diameter ratio, p/D, number of holes, n, and porosity, ϕ, of the perforation patterns are tabulated in Table 3 to summarise the geometric properties of the patterns. The given porosity was defined as a ratio of the perforated area to the solid area as described in equation (3.1)

$$\phi = \frac{nd^2}{4DL_3} \tag{3.1}$$

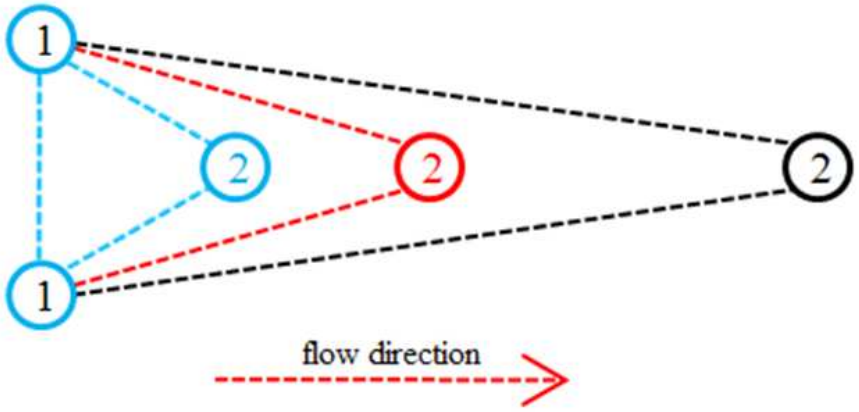

Figure 14: Variation in perforation pattern longitudinal spacing

Pattern	Perforation	p [mm]	p/D [-]	n [-]	ϕ [-]
1	Fine pitch	7.8	0.375	714	0.0965
2	Medium pitch	15.6	0.750	371	0.0502
3	Coarse pitch	31.2	1.500	182	0.0246

Table 3: Properties and features of the perforation patterns

3.4 Scope of Experiments

Experiments were conducted in the turbulent flow regime under adiabatic conditions and the injection ratio of the experiments was defined by equation (3.2). The parameter, *Q*, represented the flow rate measured by the flow meter on the main line and, *q*, was the flow rate measured by the flow meter on the injection line. The injection ratio was varied from 0 to 5% in increments of 1% while the outlet Reynolds numbers were varied from 20 000 to 60 000 at a resolution of 5 000. A total of 135 unique combinations of pitch-diameter ratio, outlet Reynolds number and injection ratio were tested to obtain friction factor data points at low injection ratios. Thus, the friction factors were obtained for different perforation pitches, injection ratios and Reynolds numbers. The scope of the experiments is summarised in Figure 15.

$$r_Q = \frac{q}{Q+q} \tag{3.2}$$

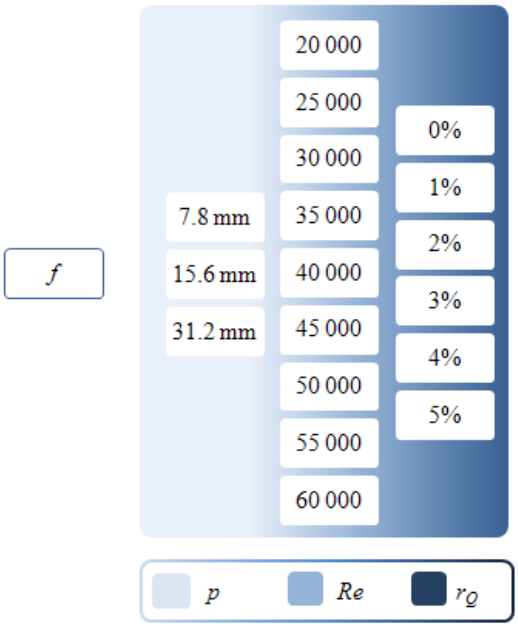

Figure 15: Summary of the scope of the experiments

3.5 Data Acquisition and Reduction

The measurements were recorded under steady-state conditions for a given perforation pitch spacing at the desired Reynolds number and injection ratio. Sixty data points for four thermocouple readings, pressure drop measurements and main or injection line flow rates were logged at a frequency of 2 Hz. Thus, a total of 120 data points for temperature and pressure drop were logged for sets containing both main and injection line flow rate data.

The recorded data was reduced after completing five major milestones. These milestones were determining fluid properties as a function of average fluid temperature, total flow rate at the tube outlet, Reynolds number, injection ratio and then calculating the friction factor. The four thermocouples mounted on the mixer of the outlet of the test section were used to complete the first milestone of determining the average fluid temperature. The readings were averaged using equation (3.3) and then the average temperature, T, was used to obtain the average fluid viscosity and density at temperatures close to 20°C.

$$T = \frac{1}{240}\sum_{i=1}^{60} T_{1\,i} + T_{2\,i} + T_{3\,i} + T_{4\,i} \tag{3.3}$$

The second milestone involved calculating the flow rate at the outlet of the test section from the main and injection line flow rate measurements. The outlet flow rate, Q_o, was the sum of the main flow rate, Q, and injection line flow rate, q. The net flow rate was then used to calculate both the Reynolds number and injection ratio for the third and fourth milestones.

The Reynolds number was calculated from equation (3.4) using the outlet flow rate, Q_o, and the fluid viscosity, which was calculated from the average fluid temperature. A Reynolds number defined in this manner was ambiguous since the information about the rate of fluid injection was lost after summing the flow rates. Therefore, an injection ratio defined by equation (3.5) was introduced to describe the rate of fluid injection for a given Reynolds number. The last milestone involved reducing the pressure drop to become a dimensionless quantity. Hence, the pressure drop, outlet flow rate and fluid density were combined through equation (3.6) to define the friction factors of the experiments. Thus, Reynolds number, injection ratio and friction factor are the dimensionless outputs for the experiments of the current study.

$$Re = 4\frac{\rho Q_o}{\mu(T)\pi D} \tag{3.4}$$

$$r_Q = \frac{q}{Q_o} \tag{3.5}$$

$$f = \frac{\Delta P \pi^2 D^5}{8L\rho(T)Q_0^2} \tag{3.6}$$

3.6 Calibration and Uncertainty

The instrumentation employed for measuring the Reynolds number, injection ratio and friction factor were calibrated before being utilised. The thermocouples were calibrated against a reference temperature probe in a thermal bath. The temperature of the thermal bath was allowed to drop from 70°C to 30°C overnight. A water column was utilised to calibrate the differential pressure transducer against a certified manometer and the measurements varied between 0 kPa and 7 kPa during calibration and testing. The Coriolis flow meters installed on the main and injection line were calibrated by the manufacturer and equation (3.7) was used together with the calibration factors in Table 4 to convert the measurements into readings.

$$\beta = m\bar{\beta}_m + \beta_o \tag{3.7}$$

	Name	β	m	β_o
1	Temperature 1	T_1	0.997	0
2	Temperature 2	T_2	0.999	0
3	Temperature 3	T_3	0.998	0
4	Temperature 4	T_4	0.996	0
5	Flow rate	Q and q	225 000	-900
6	Pressure drop	ΔP	5.204	Static reading

Table 4: Measured variables and calibration factors

The uncertainty in measurement of the experimental equipment was determined from the data sheets supplied by the manufacturers. The ranges of the experiments were used together with the data sheets to determine the uncertainties of the measurements. The ranges for the main and injection line flow meters were 1 121 *l*/h to 3 543 *l*/h and 12 to 177 *l*/h respectively.

The minimum flow rate of 1 121 *l*/h on the main line equated to a Reynolds number of 20 000 with an injection ratio of 5% and the maximum flow rate of 3 543 *l*/h was aligned to a Reynolds number of 60 000 when there was no injection. The uncertainty of these measurements remained below 0.05% since these flow rates were comparable with the full scale measurement of the flow meter. The minimum injection rate of 12 *l*/h seen in the injection line corresponded to a Reynolds number of 20 000 with an injection ratio of 1%. These flow conditions resulted in an uncertainty of 0.5% but the uncertainty dropped to 0.05% as the flow rate approached 177 *l*/h. The pressure drop measurements ranged from 0.76 kPa for a Reynolds number of 20 000 to a maximum of 6.55 kPa. A maximum uncertainty of 3% was observed for measuring the pressure drop of 0.76 kPa. The range and uncertainties of the measurements are tabulated in Table 5.

	Name	Units	Range	Maximum uncertainty
1	Main line flow meter	*l*/h	1 121 – 3 543	0.05%
2	Injection line flow meter	*l*/h	12 - 177	0.5%
3	Pressure drop	kPa	0.76 – 6.55	3%

Table 5: Measurement range and uncertainty

The method of Kline and McClintock (1953) was employed to analyse the propagation of measurement uncertainties. The uncertainty of thermocouple measurements was discarded in favour of the variation of fluid properties around the ambient temperature of 20°C with a tolerance of 5°C. The experimental ranges and maximum uncertainties for injection ratio, Reynolds number and friction factor are tabulated in Table 6.

	Parameters	Range	Maximum uncertainty
1	Injection ratio	0.84% - 5.33%	0.5%
2	Reynolds number	19 437 - 60 420	14%
3	Friction factor	0.021 - 0.031	3%

Table 6: Experimental range and maximum uncertainty

3.7 Validation and Verification

The experimental set-up and data post-processing were validated by comparing the friction factors of a plain tube with the correlation derived by Haaland (White, 2008). The design of the tube-in-tube injection system was verified by comparing the friction factors in the absence of injection for the fine pitch perforation pattern with the correlation of Siwoń (1987). The experimental error, E, defined by equation (3.8), was used to compare the friction factor found in literature, f_l, with the measured friction factor of equation (3.6).

$$E = \left|\frac{f_l - f}{f_l}\right| \times 100\% \tag{3.8}$$

3.7.1 Test Set-up Validation

The validation experiments were conducted with plain tubes without any perforations for Reynolds numbers ranging from 20 000 to 60 000. The measured friction factors were plotted along with the Haaland (White, 2008) equation, which is represented by the solid blue line in Figure 16. Two separate experimental measurements are indicated in black and red. These measurements were repeatable and the average error for the validation runs against literature was 2.4% and was within the maximum uncertainty of the experiment. It can therefore be concluded that the experimental set-up replicates the results obtained in literature.

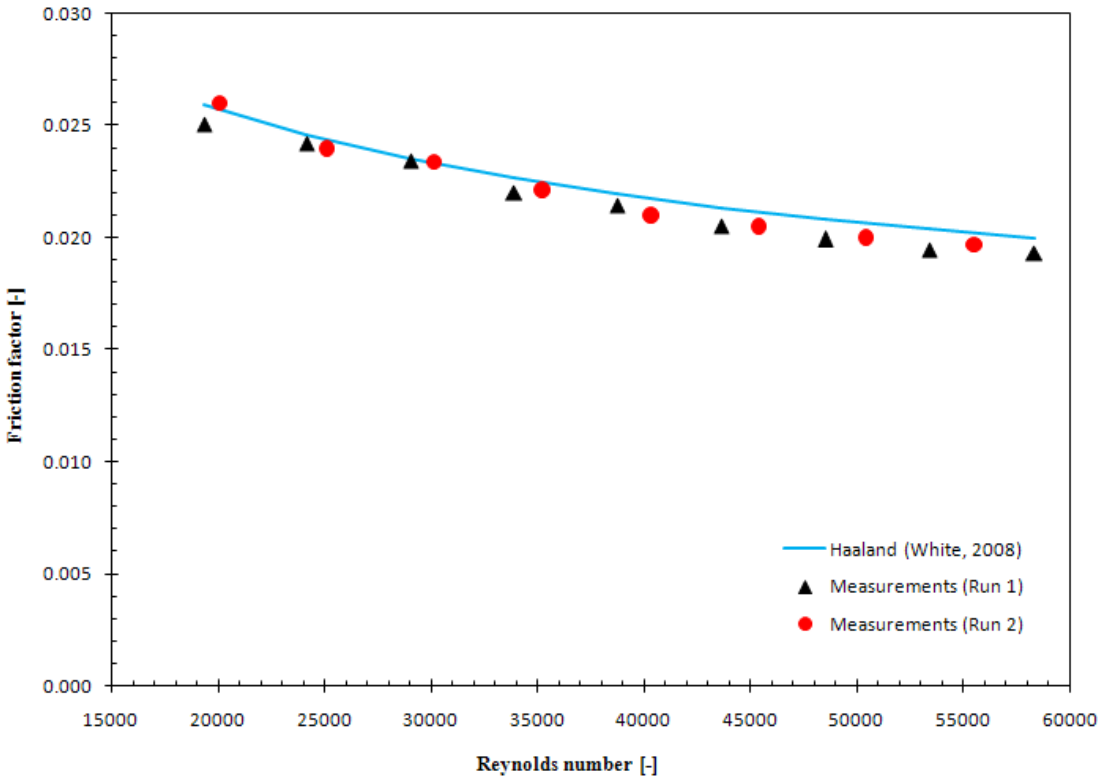

Figure 16: Experimental set-up validation with the aid of a plain tube without any perforation holes

3.7.2 Injection System Verification

The modified injection system without the perforation cover used by Su and Gudmundsson (1998) was verified to check the influence of the unregulated flow across the perforations. The fine pitch perforation pattern, which was similar to that of Siwoń (1987), was used for verifying the design of the injection system when injection was absent. Figure 17 depicts the friction factors predicted by Haaland (White, 2008) and Siwoń (1987) for plain and perforated tubes along with the experimental results, which were obtained for Reynolds numbers ranging from 19 449 to 58 574. The friction factors calculated from the plain tube correlation underpredicted both the experimental data and the correlation of Siwoń. However, there was good agreement between the correlation of Siwoń and the experimental data when the entrance and exit lengths of the perforated section were considered. The average error for the experiments was 1.3% with a maximum error of 2.7% occurring at a Reynolds number of 19 449. Hence, it can be concluded that the injection system was verified as it yielded results which were comparable with literature.

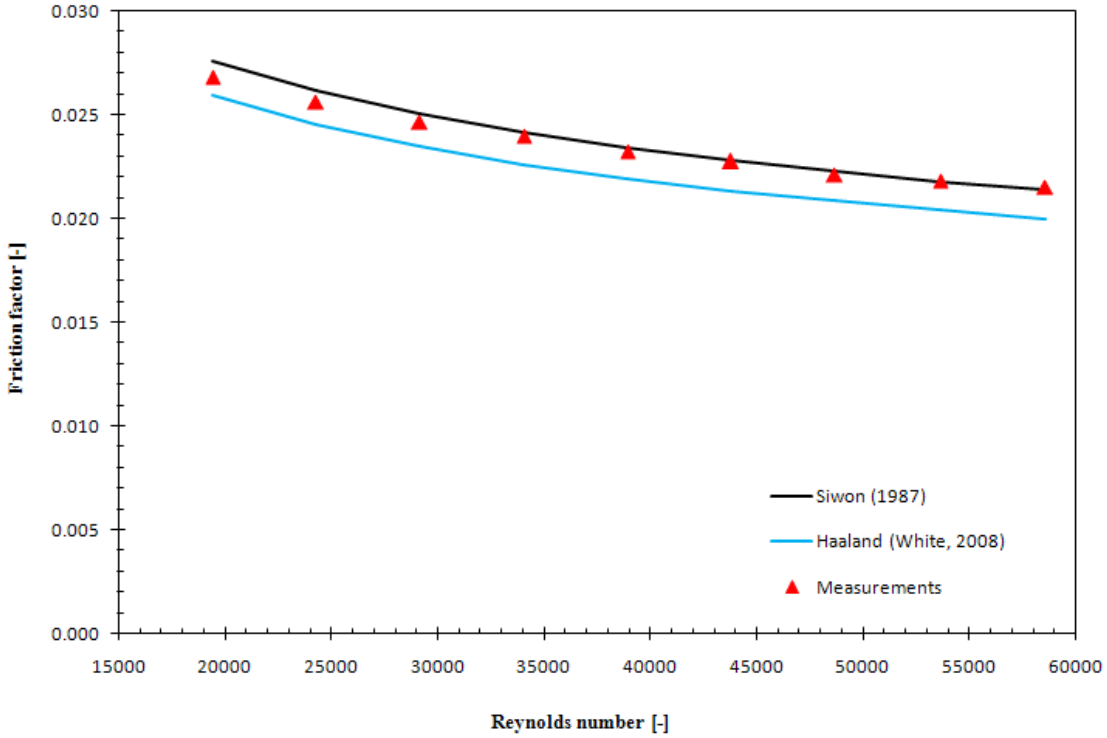

Figure 17: Injection system verification with the aid of fine pitch friction factor data in the absence of injection

3.8 Summary

The experimental set-up for conducting friction factor measurements for perforated tubes was introduced and the tube-in-tube injection system made from standard copper tubes and fittings was discussed. The major differences between the current injection system and those available in literature were described. The three perforation patterns and tubes employed in the present study were explained and graded according to pitch spacing. The scope of experiments were conducted in the turbulent flow regime with Reynolds numbers ranging from 20 000 to 60 000 and injection ratios between 0% and 5%. The experimental set-up was then used to measure plain tube friction factor data, which was found to be within 2.4% of plain tube friction factor correlations in literature. The suggested tube-in-tube injection system was also verified by comparing the experimental results of the fine pitch perforation pattern with literature. The average error for the verification experiments was found to be 1.3%. Hence, it can be concluded that the experimental set-up and injection system can be used with confidence to conduct more measurements.

4. Experimental Results

4.1 Introduction

The results for the friction factor measurements conducted on the perforated test sections are reported. The friction factors were calculated from the measured pressure drop and the results are reported either as a function of Reynolds number or injection ratio for a given perforation pattern. The experimental results indicate that injection offsets the friction factors measured in the absence of injection. Hence, the results are presented by separating zero injection friction factors from the friction factors when injection is present. The fundamental zero injection ratio friction factors are presented first and then the injection friction factors section follows afterwards.

4.2 Zero Injection Friction Factor

Zero injection friction factors were calculated from the pressure drop readings, which were obtained when the injection line was closed. Figure 18 displays friction factor values as a function of Reynolds number in the absence of injection for the fine, medium and coarse pitch perforation patterns, as well as the plain tube without any injection holes. The friction factors of the perforated tubes were higher than those of the plain tube due to perforation roughness. The effect of perforation roughness was amplified on the coarse pitch pattern (black) and less pronounced on the fine pitch pattern (blue) while the medium pitch perforation pattern (red) lies in between the two extremes.

Perforation roughness is normally directly proportional to the porosity of a perforation pattern. However, the results of the present study contradict these observations since the friction factors of the less porous pattern (coarse pitch) exceed those of the more porous pattern (fine pitch). Hence, the experimental data indicates that the friction factors of perforated tubes are directly proportional to pitch spacing for the tested cases. It can be concluded that the friction factors of perforated tubes can be reduced with maximum porosity by approaching the limit of zero pitch spacing. The limit of zero pitch spacing is a slot drilled in the direction of the flow. This result is in agreement with the use of slotted liners in the petroleum industry for horizontal oil well drilling as described by Tang (2001).

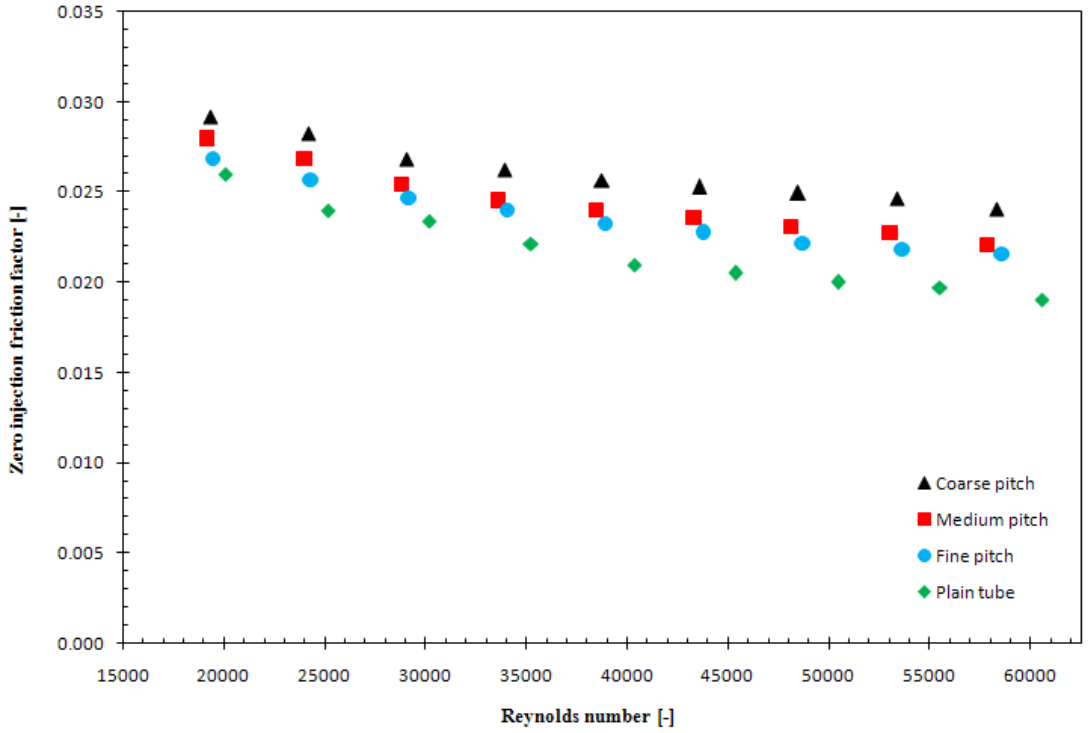

Figure 18: Friction factors against Reynolds number for a plain tube and for all the perforated tube patterns in the absence of fluid injection

4.3 Injection Friction Factor

Injection friction factors were measured when the injection line was opened and the injection flow rates were maintained to obtain the desired injection ratios. The friction factor results for the fine pitch test section at injection ratios of 0%, 3% and 5% are plotted alongside plain tube data in Figure 19a. The results reveal an increase in friction factors as the injection ratios are increased. The increase in friction was due to an upward shift of the friction factor curve and similar results were also observed for the medium pitch (Figure 19b) and coarse pitch (Figure 19c) perforation patterns. Hence, it can be concluded that injection increases the measured friction factors of perforated tubes and the increase in friction is a shift from the zero injection friction factor.

A better understanding of the effect of injection on the friction factors of perforated tubes was gained when the friction factors with injection were plotted as a function of injection ratios. The injection friction factors of the fine pitch perforation pattern are plotted in Figure 20 at Reynolds numbers of 20 000, 40 000 and 60 000.

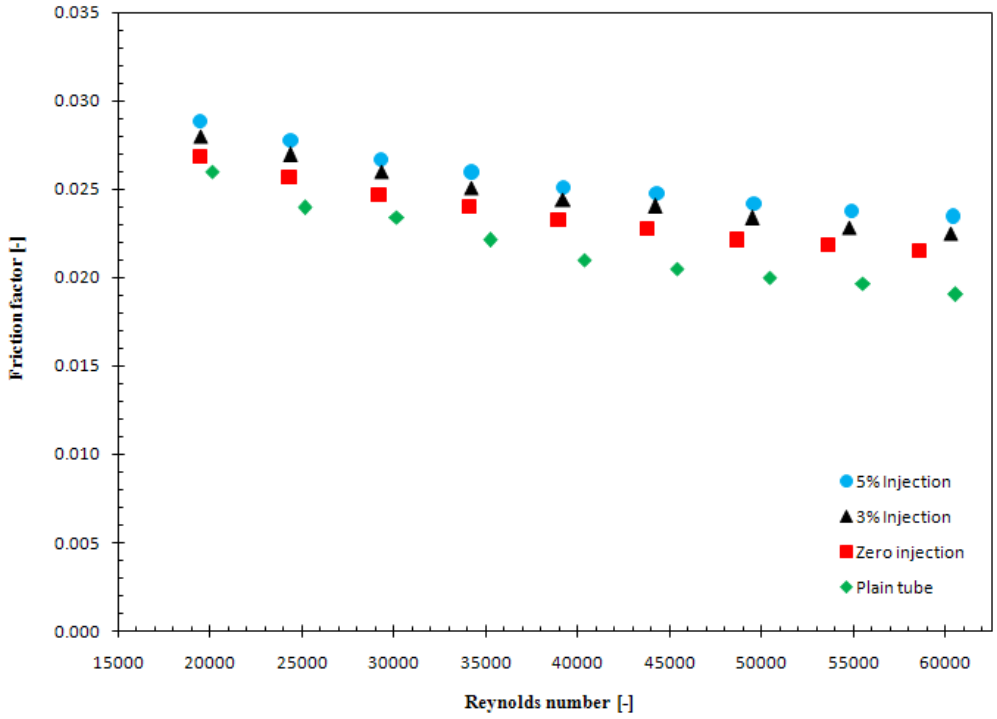

Figure 19a: Friction factor against Reynolds number for a plain tube and a fine pitch perforation pattern at different injection ratios

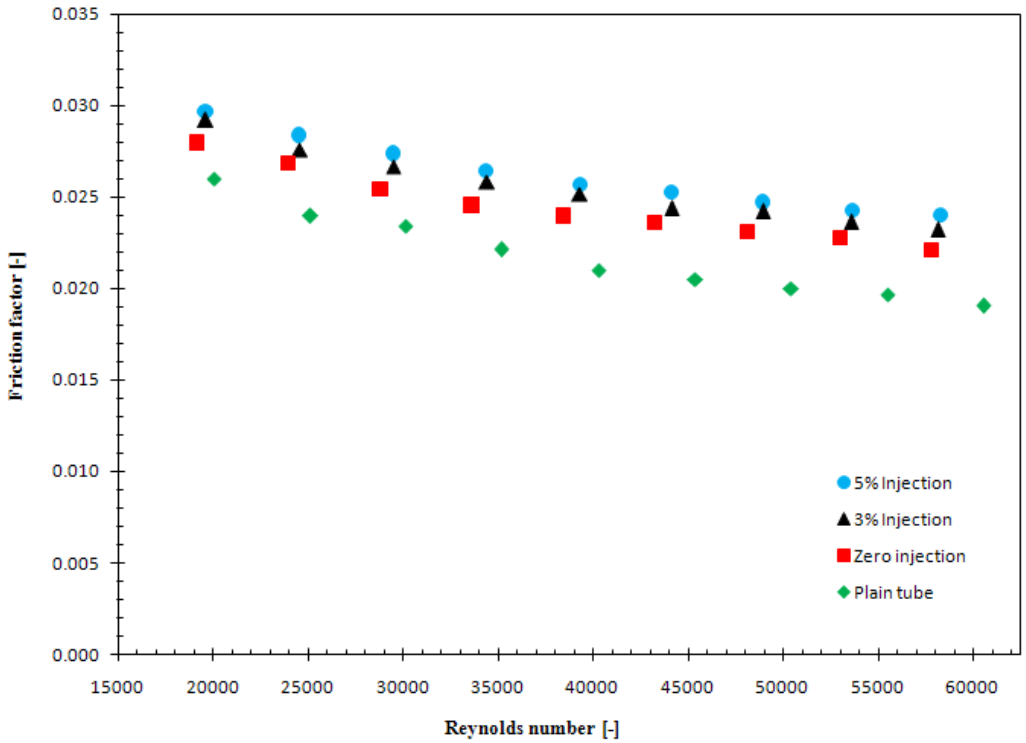

Figure 19b: Friction factor against Reynolds number for a plain and a medium pitch perforation pattern at different injection ratios

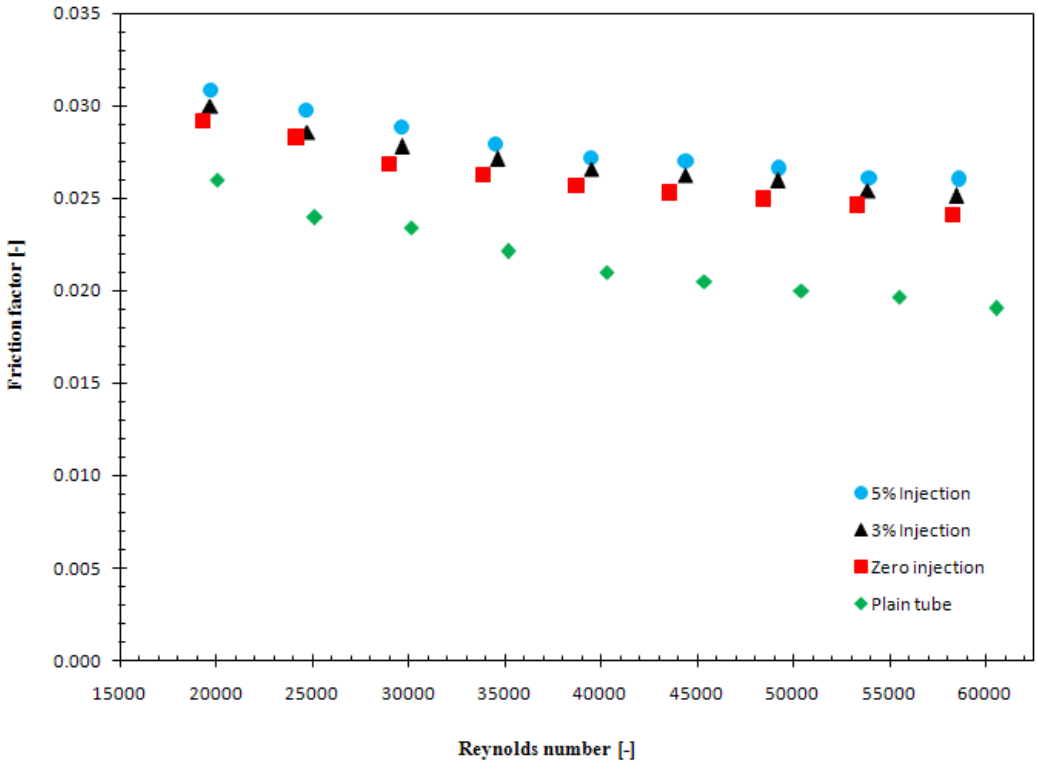

Figure 19c: Friction factor against Reynolds number for a plain tube and a coarse pitch perforation pattern at different injection ratios

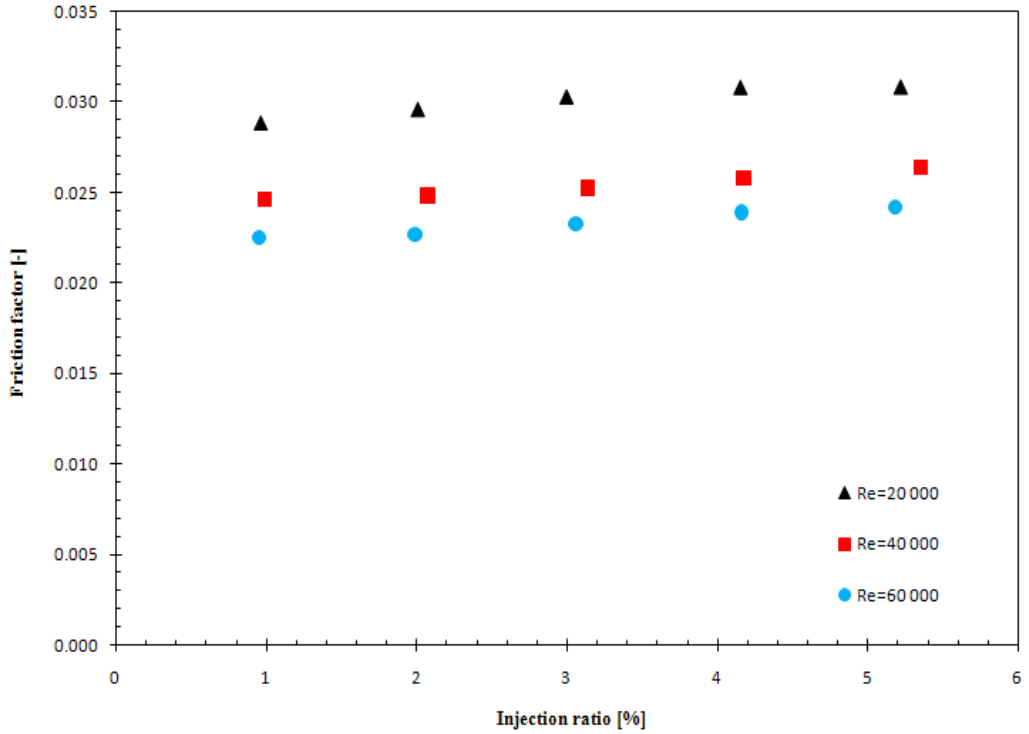

Figure 20: Friction factor against injection ratio for a fine pitch perforation pattern at Reynolds numbers of 20 000, 40 000 and 60 000

Figure 20 illustrates that the measured pressure drop and friction factor of the perforated tubes increase linearly with an increase in injection ratio. The gradient of the linear trend is independent of the Reynolds number such that the Reynolds number only governs the value of the zero injection friction factors. The zero injection friction factor act as the intercept of the injection curve with the friction factor axis yields. Hence, the value of friction factors with injection is dependent on the friction factors measured under zero injection conditions. This result implies that the friction factors of perforated tubes with injection are optimised by altering the geometry of the perforations such that lower friction factors are obtained when injection is absent.

4.4 Summary

The friction factors of perforated tubes are higher than those of plain tubes under the same flow conditions. The increase in friction was due to perforation roughness and the effect of perforation roughness was dominated by changes in pitch spacing more than porosity. Hence, the influence of perforation roughness can be reduced by varying pitch-diameter-ratio. A slot was suggested as the limit of zero perforation pitch spacing and this comment was supported by the wide use of slotted liners in the petroleum industry for horizontal oil well drilling.

The experimental results with injection reveal an increase in friction factors with an increase in injection. The increase in friction was due to an upward shift of the friction factor curve as injection the injection ratio was increased. A deeper understanding of the trend of injection was gained when the friction factors were plotted as a function of injection ratio. These results indicate that the friction factors of perforated tubes increase in a linear fashion with an increase in injection ratio. It was also noted that the increase in friction factor was a weak function of the Reynolds number and the friction factor without injection could be extrapolated from the friction factor curves with injection. It was concluded that the friction factors of perforated tubes with injection can be optimised by modifying the perforation pattern under zero injection conditions. This knowledge formed the basis of developing simplified friction factor correlations for perforated tubes with injection.

5. Discussion

5.1 Introduction

The experimental results reported in the previous chapter are condensed into correlations which can be used to determine the friction factors of perforated tubes at low injection ratios. The relationship which exists between injection and zero injection friction factors mentioned in the previous section is explained in detail and used to introduce the form of the linear friction factor correlations. The friction-reducing effects described by Su and Gudmundsson (1998) are applied to the newly developed correlations by considering the solutions of Siwoń (1987) to account for fluid acceleration caused by injection. The advantages of the newly developed correlations are demonstrated by applying the correlations to an example problem.

5.2 Friction Factor Correlations

Tang (2001) suggested a linear equation in the form of equation (5.1) to describe the friction factors as a linear function of injection ratio, r_Q. The first term, f_o, on the right-hand side describes the zero injection friction factor as a function of Reynolds number and pitch diameter ratio. The Reynolds numbers at the outlet of the tube and pitch divided by the inner diameter were used as dimensionless variables for describing the flow and perforation pattern. Then equation (5.2) was used to fit the experimental data of the coarse, medium and fine pitch perforation patterns. The constants, *a*, *b* and, *c*, for the curve fit are tabulated in Table 7. These constants predicted the friction factors within 1.5% of the measured values as shown in Figure 21.

$$f = f_o + mr_Q \tag{5.1}$$

$$f_o = aRe^b - c \tag{5.2}$$

	Perforation	*p/D*	*a*	*b*	*c*
1	Fine pitch	0.375	0.199	-0.20	7.6E-4
2	Medium pitch	0.75	0.218	-0.20	2.3E-3
3	Coarse pitch	1.5	0.157	-0.17	2.4E-4

Table 7: Zero injection friction factor prediction constants

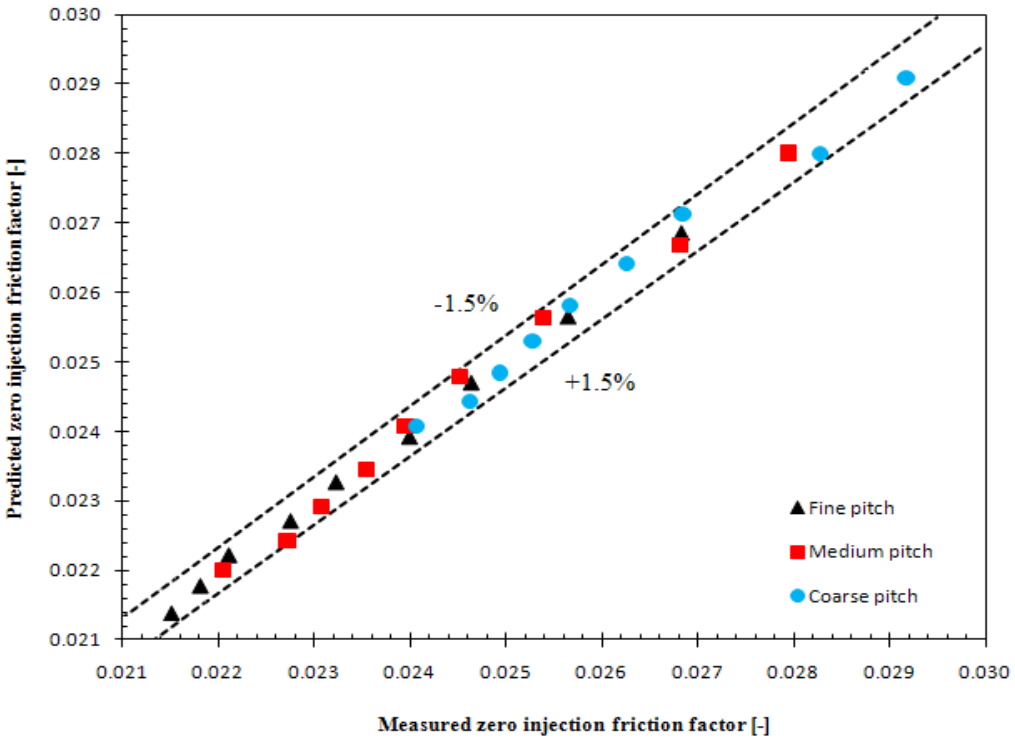

Figure 21: Measured friction factor against predicted friction factor in the absence of injection for the fine, medium and coarse pitch perforation patterns

The second term, mr_Q, on the right-hand side of equation (5.1) introduces the influence of injection once the friction factors in the absence of injection are known. Figure 22 illustrates the importance of the zero injection friction factors with the aid of the results from the fine pitch perforation pattern. The lower (20 000), central (40 000) and upper Reynolds (60 000) numbers of the testing regime were selected to demonstrate the influence of injection. The friction factors in the absence of injection were subtracted from the measured friction factors with injection and the difference was multiplied by a factor of 100 to aid interpreting the results.

A similar friction factor gradient, *m*, was observed regardless of the Reynolds number. The gradient also remained fairly constant within the narrow injection ratio range of the present study. However, the gradient was affected by pitch spacing and gradient values of 0.036, 0.030 and 0.032 were obtained for the fine, medium and coarse pitch perforation patterns respectively. The central Reynolds number of 40 000 was selected to illustrate the fit of these suggested gradients for the coarse, medium and fine pitch perforation patterns. The results were within 3% of the measured friction factors as shown in Figure 23.

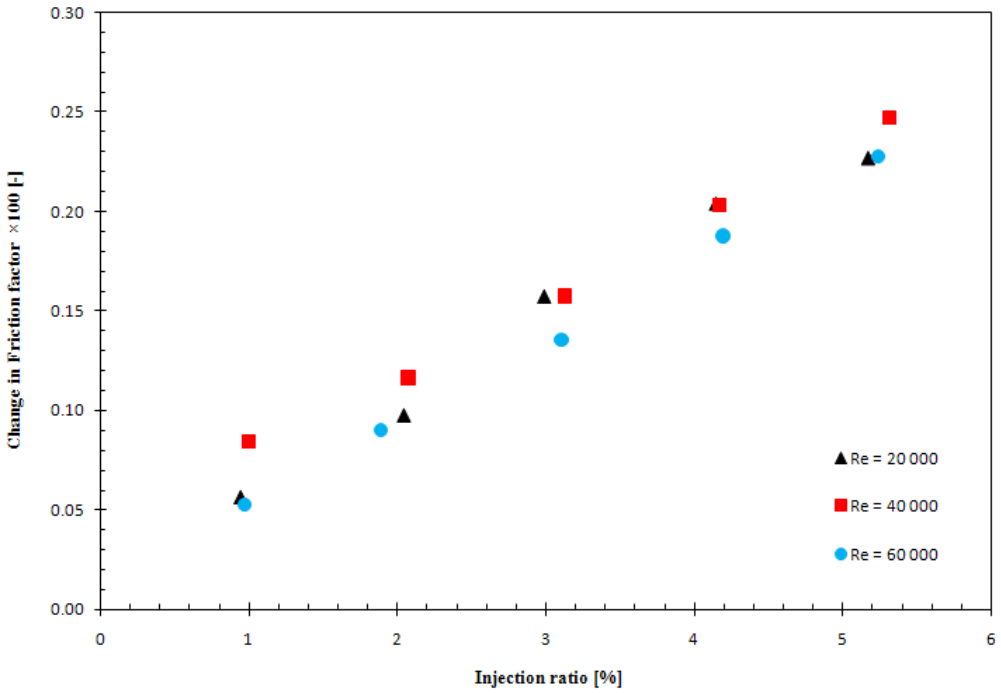

Figure 22: Linear increase in friction factor against injection ratio for a fine pitch perforation pattern at Reynolds numbers of 20 000, 40 000 and 60 000

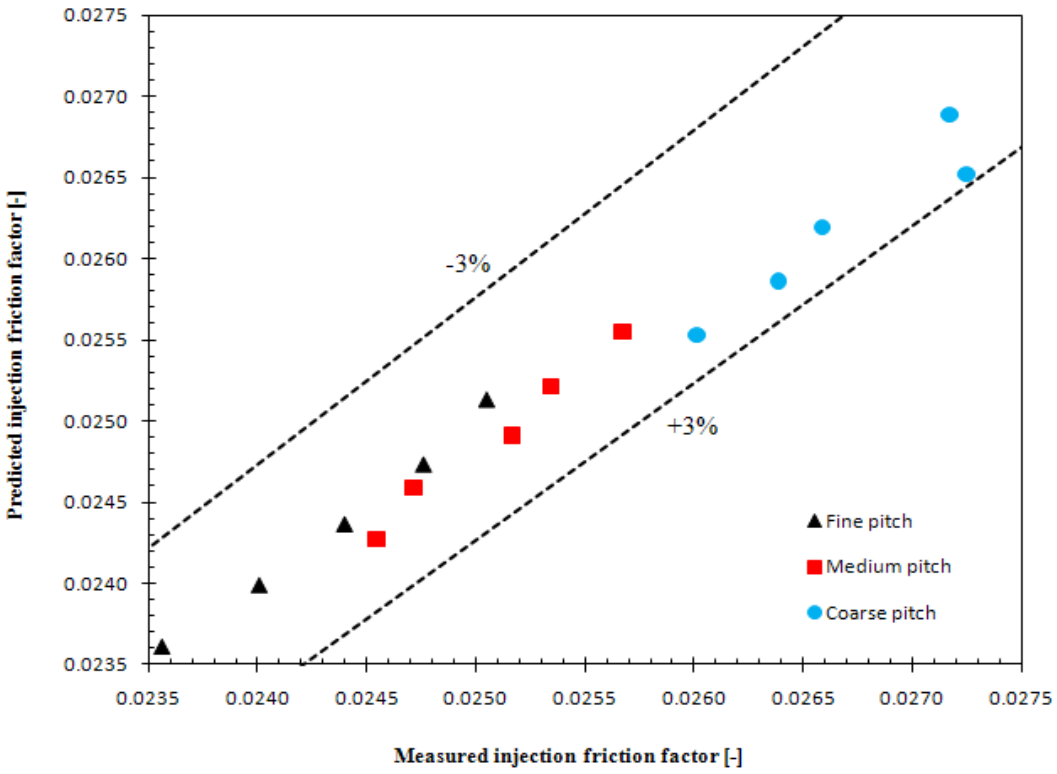

Figure 23: Measured friction factors with fluid injection against predicted friction factors at a Reynolds number of 40 000 for the fine, medium and coarse perforation patterns

5.3 Fluid Acceleration Correction

The friction factor correlations presented in the previous section are sufficient for predicting the pressure drop that would be measured across perforated tubes. However, the presence of the increased kinetic energy and fluid acceleration means a portion of the drop in pressure can be recovered. Su and Gudmundsson (1998) corrected for fluid acceleration by subtracting the kinetic energy pressure drop term defined by equation (5.3) from their pressure drop data.

$$\Delta P_k = \rho(V_2^2 - V_1^2) \tag{5.3}$$

Siwoń (1987) recommended a maximum coefficient of 0.93 for equation (5.3) instead of unity employed by the former researchers. The value of 0.93 corresponds with the peak coefficient value, c_e, of 1.86. Hence, it is desirable to combine the knowledge gained from both studies when the fluid acceleration correction term, which can be used to predict the irreversible pressure losses of a perforated tube problem. The correction term defined by equation (5.4) was introduced by applying the relationship proposed by Weisbach (White, 2008). The correction term depends on injection ratio, r_Q, and length-to-diameter ratio, *L/D*, and it is independent of the perforation pattern.

$$\Delta f = 1.86 \frac{r_Q(2 - r_Q)}{L/D} \tag{5.4}$$

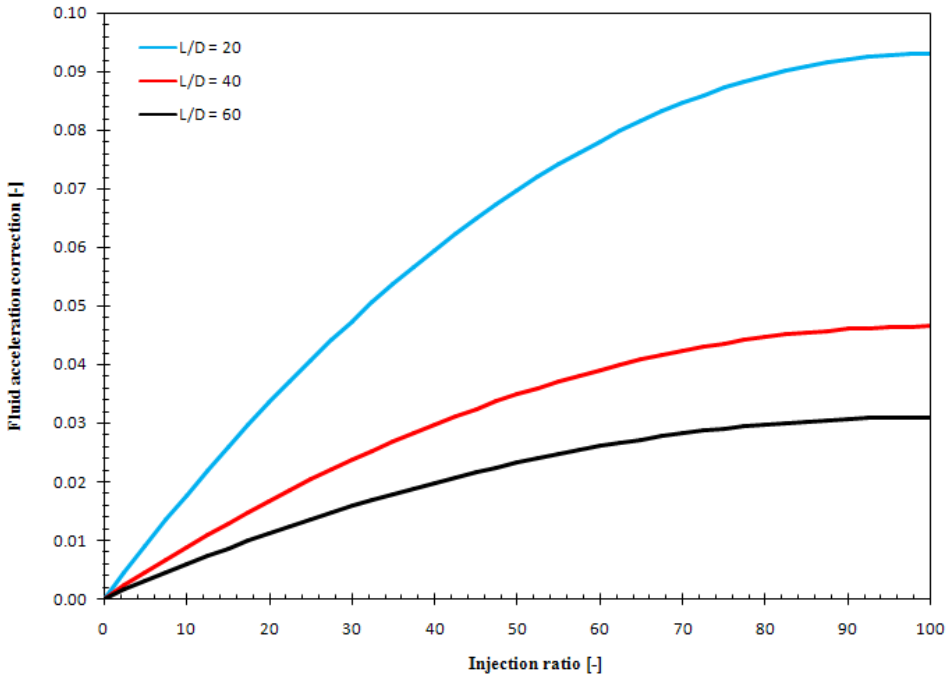

Figure 24: Fluid acceleration correction term against injection ratio at length-to-diameter ratios of 20, 40 and 60

Figure 24 illustrates the fluid acceleration correction term plotted as a function of injection ratio for three length-to-diameter ratios. The injection ratio was allowed to vary from 0% to 100% for length-to-diameter ratios of 20, 40 and 60. The figure illustrates that the fluid acceleration correction term is directly proportional to injection ratio and inversely proportional to length-to-diameter ratio. It is also clear that maximum correction is required for an injection ratio of 100% and the amount of correction is more sensitive to length-to-diameter ratio than to injection ratio. Hence, it can be concluded that the effects of fluid acceleration are more pronounced in cases where the length of the perforated tubes is relatively short and the injection ratios are fairly high.

The experiments in the present study were conducted on test sections with length-to-diameter ratio of 60 and the injection ratios ranged from 0% to 5%. The influence of the fluid acceleration correction term on the experimental results was calculated by subtracting its contribution from the friction factors which were computed from the derived correlations. The effect of the fluid acceleration correction term on the friction factors at a Reynolds number of 40 000 is depicted in Figure 25 for the fine, medium and coarse pitch patterns.

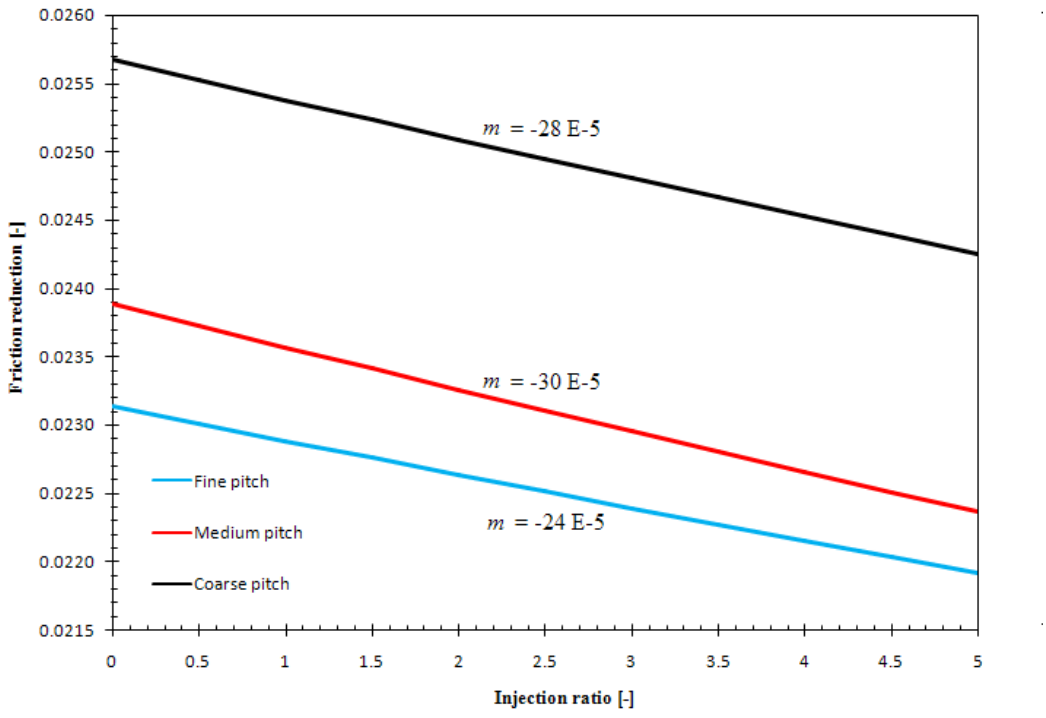

Figure 25: Effect of fluid acceleration correction term on the calculated friction factors with varying injection ratios for the fine, medium and coarse pitch perforation patterns at a Reynolds number of 40 000

Subtracting the fluid acceleration correction term affected the magnitude and sign of the gradients reported in Section 5.2 such that the friction factors of the perforated tubes are reduced with an increase in fluid injection. The corrected friction factors indicate a reduction of 13.8% (fine pitch), 13.5% (medium pitch) and 12.5% (coarse pitch) after considering the effects of fluid acceleration at an injection ratio of 5%.

The gradients of the curves changed from 0.036 to -24E-5 for the fine pitch pattern and 0.030 to -30E-5 for the medium pitch pattern while the gradient of the coarse pitch perforation pattern changed from 0.032 to -28E-5. These values indicate that the medium pitch perforation pattern is more sensitive to friction reduction than the other patterns. The superior sensitivity is due to an optimised porosity, which avoided the extreme conditions represented by the fine and coarse pitch patterns. A high porosity pattern like the fine pitch pattern is prone to injection back pressure since the perforation area is larger. On the other hand, a coarse pitch pattern has high mixing losses due to high injection speeds caused by the reduced porosity. In conclusion, the porosity of the medium pitch pattern together with the friction factors of the fine pitch pattern presents a good platform for reducing the negative effects of perforation roughness and fluid injection in perforated tubes.

5.4 Application

The application of the developed correlations to long perforated tubes with high injection ratios is demonstrated with the aid of an example. Two examples are used and the first example illustrates the use of the correlations without the correction term while the second case illustrates the effect of the fluid acceleration correction term.

5.4.1 Example 1

A perforated tube with a similar perforation pattern to the fine pitch pattern with a diameter of 100 mm was used for draining a fluid at a steady flow rate of 12 000 *l*/h. The tube was 40 metres long and 40% of the fluid entered uniformly through the perforations as indicated in Figure. The pressure drop across the perforated tube is unknown and can be calculated from the correlations which are available in literature. The correlations which are developed in the present study can also be used to determine the pressure drop across such a perforated tube when the length is divided into segments such that the injection ratio of each segment is below 5%.

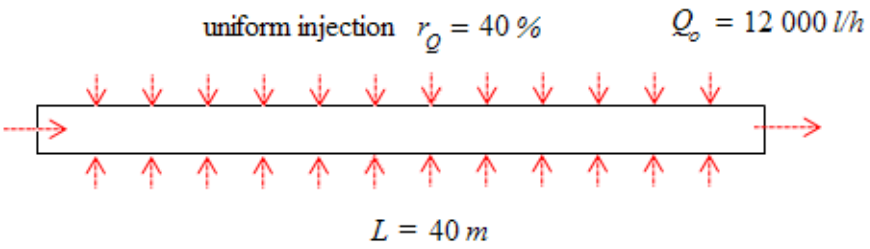

Figure 26: Schematic representation of Example 1

A seven-step method based on geometric progression was employed for discretising the length of the perforated tube. The method divides the given tube length, L, and injection ratio, r_Q, to obtain the number of segments required for an assumed low injection ratio value, r, to be valid. The output from the method is the number of segments, s, length of each segment, L_j, outlet flow rate of each section, Q_{oj}, and the injection ratio of each segment, r_j. The injection ratio of each segment is approximately equal to the assumed injection ratio such that an assumed injection ratio between 1% and 5% will allow the use of the equations developed in the present study. The outline of the segmentation method is shown in Figure 27.

Given: r_Q, Q_o and L

Assume: $0.01 < r < 0.05$

Step 1: $a_\beta = \frac{1}{1-r}$ [5.5]

Step 2: $s = \frac{\log(1-r_Q)}{\log(1-r)}$ [5.6] $s \geq 1$

Step 3: $l_1 = L\frac{1-a_\beta}{1-a_\beta^s}$ [5.7]

for $j = 1, 2, 3, \ldots, s$

Step 4: $l_j = l_1 a_\beta^{j-1}$ [5.8]

Step 5: $q_j = \frac{l_j}{L} r_Q \times Q_o$ [5.9]

Step 6: $Q_{o,j} = Q_o - \sum_{k=j+1}^{s} q_k$ [5.10]

Step 7: $r_j = \frac{q_j}{Q_{o,j}}$ [5.11]

Figure 27: Outline of seven-step length segmentation method

The injection ratio, outlet flow rate and perforated tube length were entered into a spreadsheet with an assumed maximum injection ratio of 5% per segment and 10 segments were required to maintain an injection ratio of 5% along the 40 m long length. The length, injection flow rate and outlet flow rate of each section were computed and a schematic representation of the low injection version of Example 1 is shown in Figure 28. The outlet and injection flow rate were used to determine the Reynolds number and injection ratio of each segment. These parameters were substituted into equations (5.1) and (5.2) to determine the friction factor and then equation (2.3) to obtain the pressure drop for each segment. The individual pressure drops of each segment were summed and the results are summarized in Table 8.

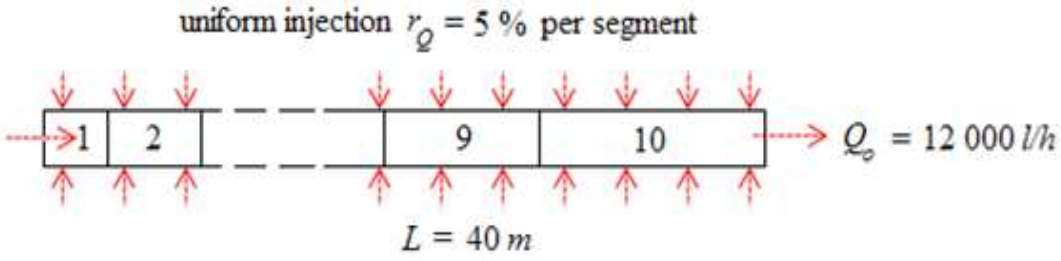

Figure 28: Schematic representation of the segmented low injection version of Example 1

	L [m]	q [l/h]	Q_o [l/h]	Re [-]	f [-]	ΔP [Pa]
1	3.14	377	7 576	26 744	0.02694	30.3
2	3.31	397	7 973	28 145	0.02667	35.0
3	3.48	418	8 391	29 619	0.02641	40.4
4	3.66	440	8 831	31 171	0.02616	46.7
5	3.86	463	9 293	32 805	0.02590	53.9
6	4.06	487	9 781	34 524	0.02565	62.2
7	4.27	513	10 293	36 334	0.02540	71.8
8	4.50	540	10 833	38 239	0.02515	82.9
9	4.73	568	11 401	40 245	0.02491	95.7
10	4.98	598	12 000	42 356	0.02467	110.5
Total	**40.00**	**4 800**	**12 000**			**629.3 Pa**

Table 8: Segmented low injection solution for Example 5.1

The suggested method allows the friction factor for injection ratios exceeding 5% to be computed from the correlations derived in the present study. Equation (5.1) and (5.2) were used along with the constant of the fine pitch perforation pattern to obtain the friction factor and pressure drop of the perforated tube. The correlation of Siwoń (1987) predicts a pressure drop of 692.8 Pa, which is within 9.2% of the 629.3 Pa computed from the low injection ratio correlations. The under prediction error is partly due to the perforation entrance and exit lengths. The entrance and exit length of each segment creates smooth sections along the segmented pipe, which are absent in the original pipe. Hence, compensation for these sections is paramount.

Deriving a single compensation equation for the correlations presented in section 5.2 is a complex process since the friction factors for the plain and perforated sections do not have an additive relationship. However, an additive relationship exists for the pressure drop measurements. This implies that the friction factor correlations developed in this study can be used to determine the pressure drop over the entire test length with plain sections included, and the pressure drop of the plain section can be subtracted from this value.

The Halaand friction factor correlation (White, 2008) was used to predict the pressure drop over the plain sections due to the reasonable agreement between the data and correlation (section 3.7.1). Thus, the pressure drop term, which remained after subtracting the losses experienced in the plain sections, was used to develop friction factors constants, which compensate for the plain sections. The friction factor compensation constants obtained from the calculations are tabulated in Table 9. These constants predict a pressure drop of 744.5 Pa for example 5.1, The pressure drop is 7.4% higher than the value predicted using the correlations, which are available in literature. Thus, it can be concluded that the results obtained under low injection have sufficient resolution such that a high injection ratio solution can be approached when small increments are used.

	Pattern	*p/D*	*a*	*b*	*c*	*m*
1	Fine pitch	0.375	0.198	-0.19	-8.1E-6	0.063
2	Medium pitch	0.75	0.250	-0.21	-1.2E-5	0.053
3	Coarse pitch	1.5	0.140	-0.15	-1.3E-4	0.058

Table 9: Friction factor compensation constants for accounting for the plain tube sections

5.4.2 Example 2

An ideal diffuser was added to the outlet of the perforated tube explained in Example 1 such that the fluid acceleration correction term of equation (5.4) is applicable. The diffuser requires a diameter ratio of 1.3 with an outlet diameter of 130 mm. The velocity at the inlet of the perforated tube was then made equal to the velocity at the outlet of the diffuser. The friction factors of the segments listed in Example 1 were calculated from equation (5.12) when a diffuser was present. These friction factors were then used to obtain the pressure drop of each segment.

$$f_D = f - \Delta f \tag{5.12}$$

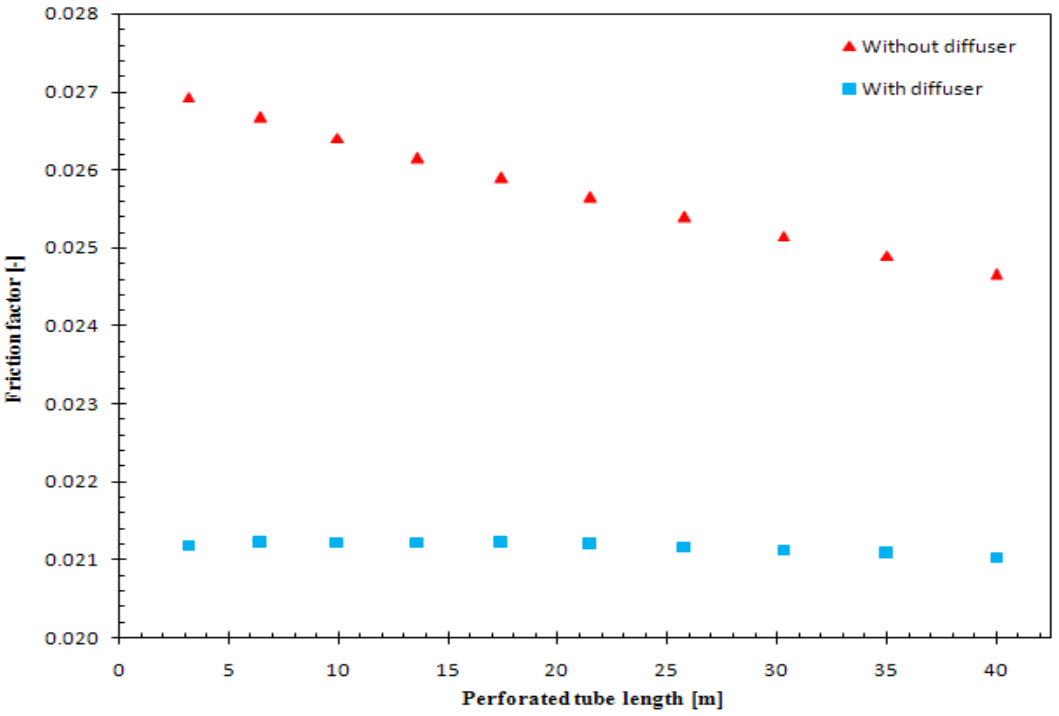

Figure 29: Influence of a diffuser on the friction factor of local segments along the length of a perforated tube which is divided into 10-segments

The friction factors obtained in Example 1 and after installing a diffuser are plotted in Figure 29 for all the segments along the perforated tube length. The friction factor curve remains fairly flat when a diffuser is present and a large portion of the reduction in friction occurs at the inlet due to a higher injection ratio per unit length. The reduced friction causes a 17% reduction in pressure drop with a net pressure drop of 522.3 Pa after installing the diffuser. The pressure drop and friction factors for both cases are summarised in Table 9.

	Without diffuser		Correction	With diffuser	
	ΔP [Pa]	f [-]	Δf [-]	f_D [-]	ΔP_D [Pa]
1	30.3	0.02694	0.0057	0.02119	23.9
2	35.0	0.02667	0.0054	0.02122	27.8
3	40.4	0.02641	0.0052	0.02123	32.5
4	46.7	0.02616	0.0049	0.02123	37.9
5	53.9	0.02590	0.0047	0.02122	44.1
6	62.2	0.02565	0.0044	0.02120	51.2
7	71.8	0.02540	0.0042	0.02117	59.8
8	82.9	0.02515	0.0040	0.02113	69.6
9	95.7	0.02491	0.0038	0.02109	81.0
10	110.5	0.02467	0.0036	0.02104	94.2
Total	**629.3 Pa**				**522.3 Pa**

Table 10: Influence of the fluid acceleration correction term per segment due to a diffuser

5.5 Summary

The experimental measurements obtained under low injection ratios were condensed into linear friction factor correlations where the injection contribution was separated from the influence of the Reynolds number. The friction factor under no injection condition for the three perforation patterns can be predicted within 1.5% of the experimental results and the proposed gradients allow the friction factors with injection to be predicted within 3% of the experimental results. The effect of fluid acceleration associated with fluid injection was considered by introducing the fluid acceleration correction term, which is dependent on injection ratio and length-to-diameter ratio. The effects of length-to-diameter ratio are more dominant than those of the injection ratio and a reduction in friction can be achieved by decreasing the length-to-diameter ratio and increasing the injection ratio. The newly developed correlations were applied to example problems to demonstrate the application of the correlations under high injection rate flow conditions. A seven-step method of segmenting the perforated tube allowed the injection ratio to remain below 5% and predicted a pressure drop that is within 9.2% of the results in literature. The prediction was improved to 7.5% after compensating for the smooth sections. The irreversible losses were also reduced by 17% when assuming that the fluid acceleration correction term is valid.

6. Conclusion and Recommendations

6.1 Summary

Perforated tubes are used for various applications in industry. A special application arises when there is lateral inflow into the perforated tubes. Such conditions are encountered during horizontal oil well drilling or when perforated tubes are used in French drains. The friction factors and pressure drop experienced under these conditions deviate from the friction factors and pressure drop expected for plain tubes. Several correlations are available in literature. However, the correlations are based on friction data, which spans over large injection ratios and there is insufficient resolution at low injection ratios. In addition to the low resolution, the effects of fluid acceleration are expressed as a pressure loss coefficient, which is not directly related to friction factor. Hence, the purpose of the present study was to measure the friction factor of three different perforation patterns at low injection ratios and develop friction factor correlations which have the ability to account for the effects of fluid acceleration such that the pressure drop across perforated tubes with injection can be reported in a familiar dimensionless form.

An experimental set-up consisting of a water reservoir, pumps and accumulators, rotameters, Coriolis flow meters, filters, perforated tube test section and a flow mixer were used for conducting friction factor measurements on perforated tubes at low injection ratios. The test sections were manufactured from standard tubes and fittings. A simplified tube-in-tube injection system with parallel flow was employed for injecting water into the perforated tube. The perforated tubes had an inner diameter of 20.8 mm and a length of 1.7 m. The tube length was divided into five segments and the test length was 1 225 mm long. The test length contained an 800 mm long perforated section. A staggered perforation pattern with seven holes spaced evenly around the circumference of the tube was used. Three different perforation patterns were derived by varying the pitch of the perforations. The patterns were graded fine, medium and coarse with pitches of 7.8 mm, 15.6 mm and 31.2 mm respectively. The experiments were conducted under turbulent flow conditions under adiabatic conditions with Reynolds numbers ranging from 20 000 to 60 000 at 5 000 increments. The injection ratio was varied from 0 to 5% at steps of 1% and a total of 135 unique combinations of pitch-diameter ratio, outlet Reynolds number and injection ratios were tested.

The experimental set-up was validated by comparing the friction factor data of a plain tube without perforations with the correlations which are available in literature. The experimental measurements were within 2.4% of the results in literature and it was concluded that the experiments gave good results. Hence, the experimental set-up was used to verify the performance of the injection system in the absence of injection and an average deviation of 1.4% was recorded. Thus, confidence was gained in the experimental set-up and injection system and more experiments with different perforation patterns and injection ratios were conducted.

The experiments indicated that perforated tubes have a higher friction factor than plain tubes. The friction factor increased with an increase in pitch. Hence, the friction factors of the coarse pitch perforated tube were consistently higher than the friction factor of both the medium and fine pitch test sections for similar flow conditions. An increase in friction factor with an increase in injection ratio was observed for all perforation patterns. The increase in friction factor showed a linear trend with respect to injection and the friction factor line intercepted the friction factor axis at the value of zero injection. This property was manipulated to derive friction factor correlation where the influence of the Reynolds number was separated from the influence of injection. The zero injection friction factors were the constants of the linear equations and the gradient varied from perforation pattern to perforation pattern.

A fluid acceleration correction term was introduced. The term combined the effects of fluid acceleration with the known results in literature and a correction term, which is a function of injection ratio and length-to-diameter ratio, was obtained. The influence of the correction term on the overall friction factor is increased by increasing the injection ratio and/or decreasing the length-to-diameter ratio of the perforated tube. The acceleration correction term is more responsive to changes in the latter variable than injection ratio. These correlations were then applied to an example where the injection ratio exceeds 5% and the solution was found by employing the seven-step segmentation method where the injection ratio of each segment remained below 5%. The result was within 9.2% of the results obtained with a high injection ratio correlation. The prediction error can be reduced to 7.5% after compensating for the smooth sections, which were present in the test length. An additional example demonstrated the use of the fluid acceleration correction term when a diffuser is installed. A 17% reduction in losses was observed under these conditions.

6.2 Conclusions

The experimental results indicate that the friction factor of perforated tubes is dependent on the perforation pattern. It is understood that increasing the porosity of the perforation pattern will increase the friction factor. However, the results obtained from the present study indicate that pitch spacing is more dominant than porosity. It was also observed that the friction factors measured in the absence of injection influence the friction factors measured when injection is present. Hence, the friction factors of perforated tubes with injection can be reduced by altering the distribution of the perforations.

Increasing the injection ratio resulted in an increase in the pressure drop measured across the perforated, tube. The increase in pressure drop and friction factor was a result of fluid acceleration which is related to the injection process. The energy is usually lost when a sudden expansion is used at the perforated tube outlet. However, installing a diffuser leads to a recovery of the kinetic energy and a reduction in losses as the injection ratio is increased.

6.3 Recommendations

The results show a reduction of perforation roughness effects as the pitch spacing approaches zero. The limit of such a case occurs when the perforations collapse into a slot, which is simpler and more affordable to machine.

An experimental set-up which allows for direct shear stressmeasurements would be more beneficial than the pressure drop measurements used in this study since the latter is subject to fluid acceleration effects. Hence, measuring the wall stress would develop a deeper understanding of the influence of lateral inflow on the wall friction of perforated tubes.

Lastly, peak reduction in the friction factors of perforated tubes with injection occurs at the highest possible injection ratio as the length-to-diameter ratio approaches zero. Hence, injecting fluid through a slotted perforated tube with a relatively short length-to-diameter ratio creates a foundation for an interesting study.

7. References

Clemo, T., 2010. Coupled Aquifer-Borehole Simulation. Ground Water, 48(1): 68-78.

Dikken, B.J., 1990. Pressure Drop in Horizontal Wells and Its Effect on Production Performance. Journal of Petroleum Science and Engineering, November: 1426-1433.

Eckert, E.R.G., Lombardi, G., Sparrow, E.M., 1973. Experiments on Heat Transfer to Transpired Turbulent Pipe Flows. International Journal of Heat and Mass Transfer, 17: 429-437.

Ghajar, A.J., Tam, L.M., 1997. Laminar-Transition for Forced and Mixed Convective Heat Transfer Correlations for Pipe Flows with Different Inlet Inlet Configurations. American Society of Mechanical Engineers, 181: 15-23.

Kato, H., Muira, K., Yamaguchi, H., Miyanaga, M., 1998 Experimental Study on Microbubble Ejection Method for Frictional Drag Reduction. Journal of Marine Science and Technology, 3:122-129.

Kays, W.M., 1971. Heat Transfer to the Transpired Turbulent Boundary Layer. International Journal of Heat and Mass Transfer, 15: 1023-1044.

Kline, S.J., McClintock, F.A., 1953. Describing Uncertainties in Single-Sample Experiments. Mechanical Engineering, 75(1): 3-8.

Meyer, J.P., Olivier, J.A., 2011. Transitional Flow Inside Enhanced Tubes for Fully Developed and Developing Flow with Different Types of Inlet Disturbances: Part I – Adiabatic Pressure Drops. International Journal of Heat and Mass Transfer, 54: 1587-1597.

Rathgeber, D.E., Becker, H.A., 1983. Mixing Between a Round Jet and a Transverse Turbulent Pipe Flow. The Canadian Journal of Chemical Engineering, 61: 148-157.

Rohr, J.J., Andersen, G.W., Reidy, L.W., Hendricks, E.W., 1992. A Comparison of the Drag-Reducing Benefits of Riblets in Internal and External Flows. Experiments in Fluids, 13: 361-368.

Singh, R.K., Rao, A.R., 2009. Simplified Theory for Flow Pattern Prediction in Perforated Tubes. Nuclear Engineering and Design, 239: 1725-1732.

Siwoń, Z., 1987. Solution for Lateral Inflow in Perforated Conduits. Journal of Hydraulic Engineering, 113(9): 1117-1132.

Su, Z., Gudmundsson, J.S., 1998. Perforation Inflow Reduces Friction Pressure Loss in Horizontal Wellbores. Journal of Petroleum Science and Engineering, 19: 223-232.

Tang, Y., 2001. Optimisation of Horizontal Well Completion. The University of Tulsa, Tulsa Oklahoma.

White, F.M., 2008. Fluid Mechanics. Sixth Edition. McGraw Hill, New York.

White, F.M., 2006. Viscous Fluid Flow. Third Edition. McGraw Hill, New York.